Available online at www.sciencedirect.com
ScienceDirect
Comput. Methods Appl. Mech. Engrg. 389 (2022) 114376
Computer methods in applied mechanics and engineering
www.elsevier.com/locate/cma

A fully-discrete decoupled finite element method for the conserved Allen–Cahn type phase-field model of three-phase fluid flow system

Xiaofeng Yang[a,*], Xiaoming He[b]

[a] *Department of Mathematics, University of South Carolina, Columbia, SC, 29208, USA*
[b] *Department of Mathematics and Statistics, Missouri University of Science and Technology, Rolla, MO 65409, USA*

Received 6 August 2021; received in revised form 14 October 2021; accepted 15 November 2021
Available online xxxx

Abstract

In this article, we develop and analyze a novel fully discrete decoupled finite element method to solve a flow-coupled ternary phase-field model for the system consisting of three immiscible fluid components. Based on the L^2-gradient flow approach, the conserved Allen–Cahn type dynamics is used to describe the free interface motion, where multiple nonlocal type Lagrange multipliers are used to accurately conserve the volume of each phase. The scheme is also linear, second-order time accurate, and unconditionally energy stable, due to the combination of several effective numerical techniques, including the two-step backward differentiation scheme, finite element discretization, explicit-SAV (scalar auxiliary variable) method for handling the nonlinearity, and projection method of Navier–Stokes equation. At each time step, the non-local splitting technique only requires solving several decoupled constant-coefficient elliptic equations. The implementation issues are discussed in detail. The solvability and the unconditional energy stability of the scheme are rigorously proved. Plenty of 2D and 3D numerical simulations are carried out to numerically demonstrate the accuracy, energy stability, and applicability of the proposed scheme.

Keywords: Conserved Allen–Cahn model; Phase field; Three-phase flows; Finite element method; Fully discrete scheme; Unconditional stability

1. Introduction

The mathematical modeling and numerical simulation of the three-component immiscible and incompressible fluid system using the diffusive interface (phase-field) method begin with a series of pioneering works in [1–4]. Its basic modeling framework is to use three independent phase-field variables to label the three immiscible fluid components separately, and then assume the total free energy as the combination of the respective hydrophobic (double-well potential) and hydrophilic (gradient potential) effects of each fluid component. The system not only needs to consider that the surface tension between every two fluid components may be different but also needs to include some special cases (e.g., the so-called "total spreading" when some coefficients of the gradient potential might be non-positive). Therefore, to make the entire system always be well-posed, a common practice is to add an additional energy potential to the total free energy, which is formulated as a sixth-order polynomial function involving all three phase-field variables, cf. [1,2]. In this way, as long as the specific consistency conditions of the

* Corresponding author.
E-mail addresses: xfyang@math.sc.edu (X. Yang), hex@mst.edu (X. He).

https://doi.org/10.1016/j.cma.2021.114376
0045-7825/

surface tension parameters are satisfied, the partial differential equation (PDE) system can always maintain the law of energy dissipation.

Although the use of this sixth-order polynomial potential can bring a good energy dissipation property to the three-phase system, it also brings additional numerical challenges in designing energy stable algorithms. This is because formally, this term couples the three phase-field variables very closely together in a nonlinear manner. Through long-term exploration, so far, some unconditionally energy stable methods for the three-phase model have been developed, including the Invariant Energy Quadratization (IEQ) [5] and Scalar Auxiliary Variable (SAV) [6,7] methods, the convex splitting method [8], semi- or fully-implicit method [2–4], etc. Among them, the semi-implicit, IEQ, SAV methods are second-order time accurate, while the convex-splitting is first-order time accurate. The semi-implicit [2,3] and convex splitting method [8] are both nonlinear and coupled type, where the multiple phase-field variables are coupled in a nonlinear manner, resulting in relatively high computational costs at each time step. The IEQ method [5] has linear structure. But it is still a coupled type method. The SAV method [6,7] is both linear and fully-decoupled.

It should be pointed out that most of the numerical schemes mentioned above (IEQ, SAV, convex-splitting) are developed for the reduced version of the three-phase fluid flow model, i.e., the situation without coupling the flow field. This is because the complexity of the three-phase model itself is already very high. Hence it is natural to consider the algorithm design for the reduced version first. When the flow field is involved, the model turns to a highly coupled complex form, which brings great difficulties to the design of an easy-to-implement numerical scheme. There may be some intuitions that one only needs to simply combine the method of dealing with the no-flow model and the method of dealing with the Navier–Stokes equations (e.g., the projection/Gauge/penalty methods, etc., cf. [9–15]) to successfully obtain the desired scheme. But the reality is opposite. The simple stacking idea can indeed produce some numerical schemes. However, when considering to achieve some desired features, such as temporal second-order accuracy, full decoupling, linearity, and energy stability, then the numerical scheme design will become very challenging.

To understand the difficulty of this problem more clearly, we emphasize that there exist substantial differences between the following two types of schemes, one is the "*second-order time accurate and fully-decoupled*" scheme, and the other is the "*second-order time accurate, fully-decoupled, and energy-stable*" scheme. It seems that there is not much difference between these two types of schemes, and the latter only emphasizes stability more. But in fact, there exist huge differences in the difficulty of achieving these two schemes. For example, the former can be obtained as long as the second-order temporal discretization is used for all terms. However, after the energy stability requirement is considered, it will no longer be possible to arbitrarily discretize coupled nonlinear terms to reach both second order and unconditional energy stability, because the premise of adopting any discretization method has become whether the provable energy stability can be guaranteed.

After clarifying the difference between these two types of schemes, we immediately discover that the main challenge in designing a full decoupling scheme is about how to discretize the advection and surface tension terms, since it is these two terms to couple the phase-field equations and fluid equations together. Here, we summarize the available numerical schemes according to the temporal discretization techniques of these two terms. So far, there are mainly five different methods that can achieve the energy stability, including the fully-implicit method (cf. [16,17]), the implicit–explicit method (cf. [18–22]), fully-explicit method (cf. [23]), the stabilized-explicit method (cf. [24–27]), and the explicit-auxiliary variable method [28]. The fully-implicit method leads to a nonlinear and fully-coupled scheme. The implicit–explicit method can generate a linear scheme, and even a second-order time-accurate scheme (for the matched-density case), but the resulted scheme is still fully-coupled. In [21,22], the unconditional energy stability is achieved only for the semi-discretization scheme, while the spectral method is used for the spatial discretization in the numerical experiments. The fully-explicit scheme can achieve a full decoupling structure, however, it can only obtain conditional energy stability on the time step, see [23]. The explicit-stabilization method [24–27] and the explicit-auxiliary variable method [28] are the only numerical methods that have fully-decoupled structure while ensuring unconditional energy stability. However, the explicit-stabilization method is only first-order accurate in time. In [28], which considers the Cahn–Hilliard equation, the unconditional stability of the explicit-auxiliary variable method is achieved only for the semi-discrete scheme in which the space is assumed to be continuous, while the spectral method is used for the spatial discretization in the numerical experiments.

Therefore, in this article, we aim to construct a fully discrete finite element method to solve the flow-coupled three-component phase-field model. We first replace the classic flow-coupled three-phase Cahn–Hilliard model,

which was developed in [1–3], by a relatively simpler conserved Allen–Cahn equation, where multiple nonlocal Lagrange multipliers are added so that the volume of each phase can be conserved accurately. This is a well-known effective volume-preserving method for the L^2-gradient flow model originated from [29], and has been applied in various models (especially two-phase case), see [30–39]. There also exist many works for handling the nonlinearity in the phase field models, including the convex-splitting method [40–45], the implicit quadrature method [46], the stabilization method [27,47–49], the IEQ method [50–53], the scalar auxiliary method (SAV) method [53–55], etc. Finite element methods have also been developed to solve various phase field models [56–68].

After the new flow-coupled three-component phase-field model is formulated, we aim to design the first fully discrete finite element scheme for it. More importantly, we expect that the scheme can follow the following five properties: *(i) it has a fully-decoupled structure; (ii) it is second-order time accurate; (iii) it is unconditionally energy stable; (iv) it only needs to solve linear equations at each time step; and (v) it only needs to solve equations with constant coefficients, thereby saving the extra computational cost caused by handling variable coefficients.*

To this goal, inspired by the semi-discrete version of the explicit-auxiliary variable method developed in [28] and the finite element method for spatial discretization [69], this article proposes a fully discrete numerical scheme to deal with the flow-coupled version of the ternary phase-field model. Its key idea to handle the time marching is the introduction of two auxiliary variables and the corresponding special ordinary differential equations (ODEs). Using these tools, the original system is then reformulated into an equivalent form by using an ingenious coupling method. Here, we highlight that the newly obtained PDE system is completely equivalent to the original system in the continuous level. When the new system is properly discretized, the discretized ODE plays a key role in achieving the full decoupling structure while maintaining the provable unconditional energy stability. The advantage to achieve an equivalent system for the original model is that the property of unconditional energy stability can be easily obtained by using simple explicit methods to discretize nonlinear terms. The nonlocal auxiliary variable can also be used to decompose every discrete equation into several sub-equations with constant coefficients, so that each variable can be solved independently at each time step, thereby greatly improving the computational efficiency. We further strictly prove the solvability of the scheme and its unconditional energy stability, and conduct various numerical examples to demonstrate the stability and accuracy numerically. Moreover, the proposed algorithm design framework is also applicable for establishing efficient numerical schemes to solve other coupled systems with high nonlinearity, including the hydrodynamics-coupled model discussed here, or the magnetic field [70], electric field [71,72], etc. The developed model can be coupled with variable density/viscosity to study the drop dynamics and approximate the real world simulation more accurately [73,74].

The rest of the paper is organized as follows. In Section 2, we introduce the Navier–Stokes coupled, three-component volume-conserved Allen–Cahn phase-field model, and derive its associated PDE energy dissipation law. In Section 3, we introduce the numerical scheme, explain its implementations in detail, and prove its solvability and discrete energy dissipation law rigorously. Then we provide numerous numerical examples in Section 4 to illustrate the accuracy and stability of the developed scheme and some concluding remarks in Section 5.

2. Model system

We first formulate the Navier–Stokes coupled volume-conserved Allen–Cahn phase-field model to simulate a three-phase fluid flow system with three incompressible and immiscible fluid components. Let Ω be a smooth, open bounded, connected domain in $\mathbb{R}^d$, $d = 2, 3$. Let $\phi_i(\boldsymbol{x}, t)$ with $i = 1, 2, 3$ be the ith phase-field variable which represents the volume fraction of the ith fluid component in the three-phase mixture, i.e.,

$$\phi_i(\boldsymbol{x}, t) = \begin{cases} 1 & \text{inside the } i\text{th component,} \\ 0 & \text{outside the } i\text{th component.} \end{cases} \tag{2.1}$$

A smooth layer with the thickness ϵ is used to connect the interface between the regions of $\{\phi_i = 0\}$ and $\{\phi_i = 1\}$.

Assuming that the three-phase fluid mixture is perfect (free-leakage), thus the three unknown variables $(\phi_1, \phi_2, \phi_3)(\boldsymbol{x}, t)$ satisfy the following condition:

$$\phi_1(\boldsymbol{x}, t) + \phi_2(\boldsymbol{x}, t) + \phi_3(\boldsymbol{x}, t) = 1, \tag{2.2}$$

which can be called as the "perfect mixture" or "hyperplane link condition" or "free-leakage condition", see [1,2,25].

In this paper, we adopt the total free energy formulated in [1,2,25] for the three-component model, which considers different surface tension parameters. Hence, after coupling with the fluid momentum, the total free energy is given as

$$E(\mathbf{u}, \phi_1, \phi_2, \phi_3) = E_{kinetic} + E_{mix}, \tag{2.3}$$

where

$$E_{kinetic} = \int_\Omega \frac{1}{2}|\mathbf{u}|^2 d\boldsymbol{x}, \quad E_{mix} = \lambda \int_\Omega \frac{3\epsilon}{8}\Big(\sum_{i=1}^{3} \Sigma_i |\nabla \phi_i|^2 + \frac{12}{\epsilon} F(\phi_1, \phi_2, \phi_3)\Big) d\boldsymbol{x}. \tag{2.4}$$

Here, $\mathbf{u}$ is the fluid velocity field, λ is a positive parameter that characterizes the relative magnitude of the kinetic energy $E_{kinetic}$ and mixing energy E_{mix}, the three gradient terms of each of the phase-field variable in E_{mix} contribute to the hydrophilic type (a tendency of mixing) of interactions, the energy potential F represents the hydrophobic type (a tendency of separation) of interactions, and the parameter $\epsilon \ll 1$ is related to the width of the interface. The coefficients $\Sigma_i, i = 1, 2, 3$, which are related to the surface tension parameters among each phase, represent the "spreading" coefficient of the ith at the interface between jth phase and kth phase. In [1,2,25], it is shown that when the three surface tension parameters σ_{ij} $(\sigma_{12}, \sigma_{13}, \sigma_{23})$ verify the following conditions:

$$\Sigma_i = \sigma_{ij} + \sigma_{ik} - \sigma_{jk}, i = 1, 2, 3, \tag{2.5}$$

the three-phasic system is algebraically consistent with the two-phasic system. Note that Σ_i might not be always positive. If $\Sigma_i > 0, \forall i$, the spreading is said to be "partial", and if there exists $\Sigma_i < 0$ for some i, it is called "total". The nonlinear potential $F(\phi_1, \phi_2, \phi_3)$ is given as

$$F(\phi_1, \phi_2, \phi_3) = \frac{\Sigma_1}{2}\phi_1^2(1-\phi_1)^2 + \frac{\Sigma_2}{2}\phi_2^2(1-\phi_2)^2 + \frac{\Sigma_3}{2}\phi_3^2(1-\phi_3)^2 + P(\phi_1, \phi_2, \phi_3), \tag{2.6}$$

where

$$P(\phi_1, \phi_2, \phi_3) = \begin{cases} 3\Lambda\phi_1^2\phi_2^2\phi_3^2, & \text{for 2D}, \\ 3\Lambda\phi_1^2\phi_2^2\phi_3^2\tilde{P}, & \text{for 3D}, \end{cases} \tag{2.7}$$

Λ is a non-negative constant, $\tilde{P} = \sum_{i=1}^{3} g_\alpha(\phi_i)$, and $g_\alpha(x) = \frac{1}{(1+x^2)^\alpha}$ with $0 < \alpha \leq \frac{8}{17}$.

Assuming that the three fluid components have the matched density and viscosity, and following the modeling framework given in [1,2,25], the Navier–Stokes coupled conserved Allen–Cahn model for the three-phase fluid flow system based on the L^2-gradient flow approach is formulated as:

$$\phi_{it} + \nabla \cdot (\mathbf{u}\phi_i) = -M\frac{1}{\Sigma_i}\bar{\mu}_i, \ i = 1, 2, 3, \tag{2.8}$$

$$\mu_i = -\frac{3}{4}\epsilon\Sigma_i\Delta\phi_i + \frac{12}{\epsilon}(f_i + \beta_L), \ i = 1, 2, 3, \tag{2.9}$$

$$\mathbf{u}_t + \mathbf{u}\cdot\nabla\mathbf{u} - \nu\Delta\mathbf{u} + \nabla p + \lambda\sum_{i=1}^{3}\phi_i\nabla\mu_i = 0, \tag{2.10}$$

$$\nabla \cdot \mathbf{u} = 0, \tag{2.11}$$

where $\bar{\mu}_i = \mu_i - \frac{1}{|\Omega|}\int_\Omega \mu_i d\boldsymbol{x}$, $\mu_i = \frac{\delta E}{\lambda\delta\phi_i}$ and $\frac{\delta E}{\delta\phi_i}$ is the chemical potential, $M > 0$ is the mobility, $f_i = \partial_i F$, p is the pressure, ν represents the fluid viscosity parameter, β_L is the Lagrange multiplier to ensure the free-linkage condition (2.2) and it can be derived as $\beta_L = -\frac{1}{\Sigma_T}(\frac{f_1}{\Sigma_1} + \frac{f_2}{\Sigma_2} + \frac{f_3}{\Sigma_3})$ with $\Sigma_T = \frac{1}{\Sigma_1} + \frac{1}{\Sigma_2} + \frac{1}{\Sigma_3}$.

The initial conditions read as

$$\begin{cases} \mathbf{u}|_{(t=0)} = \mathbf{u}^0, \ p|_{(t=0)} = p^0, \\ \phi_1|_{(t=0)} = \phi_1^0, \phi_2|_{(t=0)} = \phi_2^0, \phi_3|_{(t=0)} = \phi_3^0, \phi_1^0 + \phi_2^0 + \phi_3^0 = 1. \end{cases} \tag{2.12}$$

The boundary conditions read as ($\mathbf{n}$ is the unit outward normal on the boundary $\partial\Omega$),

$$\mathbf{u}|_{\partial\Omega} = \mathbf{0}, \ \partial_{\mathbf{n}}\phi_i|_{\partial\Omega} = 0, \ i = 1, 2, 3. \tag{2.13}$$

Note that the periodic boundary conditions are also widely used in [2,3,5–8].

Remark 2.1. Different from the regular Allen–Cahn dynamics that cannot conserve the volume, three nonlocal Lagrange multiplier terms are used in $\bar{\mu}_i$ of (2.8). By integrating each side of (2.8), it is easy to see that the volume can be accurately conserved for each phase, namely,

$$\frac{d}{dt}\int_\Omega \phi_i d\boldsymbol{x} = 0, \tag{2.14}$$

which is derived by using the boundary condition (2.13) for $\mathbf{u}$. Similar volume conservation method had been used for the reduced version of three-phase model (no flow field coupled), see [7].

Remark 2.2. Remarkably, it can be proved that the system (2.8)–(2.9) with three unknown phase-field variables is equivalent to a system with only two unknown phase-field variables that read as

$$\begin{cases} \phi_{it} + \nabla\cdot(\mathbf{u}\phi_i) = -M\dfrac{1}{\Sigma_i}\bar{\mu}_i, \ i = 1, 2, \\ \mu_i = -\dfrac{3}{4}\epsilon\Sigma_i\Delta\phi_i + \dfrac{12}{\epsilon}(f_i + \beta_L), \ i = 1, 2, \end{cases} \tag{2.15}$$

and the unknown variables for the third phase (ϕ_3, μ_3, $\bar{\mu}_3$) are given by the following explicit formula:

$$\phi_1 + \phi_2 + \phi_3 = 1, \tag{2.16}$$

$$\frac{\mu_1}{\Sigma_1} + \frac{\mu_2}{\Sigma_2} + \frac{\mu_3}{\Sigma_3} = 0, \tag{2.17}$$

$$\frac{\bar{\mu}_1}{\Sigma_1} + \frac{\bar{\mu}_2}{\Sigma_2} + \frac{\bar{\mu}_3}{\Sigma_3} = 0. \tag{2.18}$$

Since the proof is quite similar to Theorem 3.1, we omit the details here.

Remark 2.3. From [1,2], the following two statements hold.

(i) For any $\xi_1 + \xi_2 + \xi_3 = 0$, there exists a constant $\underline{\Sigma} > 0$ such that

$$\Sigma_1|\xi_1|^2 + \Sigma_2|\xi_2|^2 + \Sigma_3|\xi_3|^2 \geq \underline{\Sigma}\Big(|\xi_1|^2 + |\xi_2|^2 + |\xi_3|^2\Big), \tag{2.19}$$

if and only if the following condition holds:

$$\Sigma_1\Sigma_2 + \Sigma_1\Sigma_3 + \Sigma_2\Sigma_3 > 0, \ \Sigma_i + \Sigma_j > 0, \forall i \neq j. \tag{2.20}$$

(ii) For 2D case, as long as $\Lambda > 0$, the bulk free energy $F(\phi_1, \phi_2, \phi_3)$ defined in (2.6) is bounded from below if $\phi_1 + \phi_2 + \phi_3 = 1$, and the lower bound only depends on Σ_1, Σ_2, Σ_3 and Λ. For 3D case, it is shown in [1] that the bulk energy F is bounded from below when $0 < \alpha \leq \frac{8}{17}$.

Therefore, to form a meaningful physical system, we assume that the condition (2.20) always holds throughout this paper.

We now show the model equations (2.8)–(2.11) follow a dissipative energy law. Some notations are given here. Given any two functions $\phi(\boldsymbol{x})$ and $\psi(\boldsymbol{x})$, their L^2 inner product is denoted by $(\phi, \psi) = \int_\Omega \phi(\boldsymbol{x})\psi(\boldsymbol{x})d\boldsymbol{x}$, and the L^2 norm for any function $\phi(\boldsymbol{x})$ is $\|\phi\| = (\phi, \phi)^{\frac{1}{2}}$.

We multiply the L^2 inner product with $\lambda\mu_i$ for (2.8) and take the summation for $i = 1, 2, 3$ to get

$$\sum_{i=1}^{3}\lambda(\phi_{it}, \mu_i) = -\lambda M\sum_{i=1}^{3}\frac{1}{\Sigma_i}(\bar{\mu}_i, \mu_i) \underbrace{-\lambda\sum_{i=1}^{3}\int_\Omega \nabla\cdot(\mathbf{u}\phi_i)\mu_i d\boldsymbol{x}}_{I}. \tag{2.21}$$

For the term $\frac{1}{\Sigma_i}(\bar{\mu}_i, \mu_i)$, we derive

$$\begin{aligned} \frac{1}{\Sigma_i}(\bar{\mu}_i, \mu_i) &= \frac{1}{\Sigma_i}(\mu_i - \frac{1}{|\Omega|}\int_\Omega \mu_i d\boldsymbol{x}, \mu_i) \\ &= \frac{1}{\Sigma_i}(\mu_i - \frac{1}{|\Omega|}\int_\Omega \mu_i d\boldsymbol{x}, \mu_i - \frac{1}{|\Omega|}\int_\Omega \mu_i d\boldsymbol{x}) + (\mu_i - \frac{1}{|\Omega|}\int_\Omega \mu_i d\boldsymbol{x}, \frac{1}{|\Omega|}\int_\Omega \mu_i d\boldsymbol{x}) \\ &= \frac{1}{\Sigma_i}\Big\|\mu_i - \frac{1}{|\Omega|}\int_\Omega \mu_i d\boldsymbol{x}\Big\|^2 = \frac{1}{\Sigma_i}\|\bar{\mu}_i\|^2 = \Sigma_i\left\|\frac{\bar{\mu}_i}{\Sigma_i}\right\|^2, \end{aligned} \tag{2.22}$$

since $(\mu_i - \frac{1}{|\Omega|}\int_\Omega \mu_i d\boldsymbol{x}, 1) = 0$. We take the L^2 inner product of (2.9) with $-\lambda\phi_{it}$, perform integration by parts and take the summation for $i = 1, 2, 3$ to obtain

$$-\lambda\sum_{i=1}^{3}(\mu_i, \phi_{it}) = -\lambda\frac{3}{4}\epsilon\sum_{i=1}^{3}\Sigma_i\frac{d}{dt}\|\nabla\phi_i\|^2 - \lambda\frac{12}{\epsilon}\sum_{i=1}^{3}(f_i + \beta_L, \phi_{it}). \tag{2.23}$$

We take the L^2 inner product of (2.10) with $\mathbf{u}$, performing integration by parts, we obtain

$$\frac{1}{2}\frac{d}{dt}\|\mathbf{u}\|^2 + \underbrace{\int_\Omega(\mathbf{u}\cdot\nabla)\mathbf{u}\cdot\mathbf{u}d\boldsymbol{x}}_{III} + \nu\|\nabla\mathbf{u}\|^2 - (p, \nabla\cdot\mathbf{u}) + \underbrace{\lambda\sum_{i=1}^{3}\int_\Omega\phi_i\nabla\mu_i\cdot\mathbf{u}d\boldsymbol{x}}_{II} = 0. \tag{2.24}$$

Then, by combining (2.21), (2.23), (2.24), using (2.11) for the pressure term, the equality $(\beta_L, (\phi_1+\phi_2+\phi_3)_t) = (\beta_L, (1)_t) = 0$ due to (2.16), and using (2.27) and (2.28), we derive the following identity:

$$\frac{d}{dt}E(\mathbf{u}, \phi_1, \phi_2, \phi_3) = -\nu\|\nabla\mathbf{u}\|^2 - \lambda M\underbrace{\left(\Sigma_1\left\|\frac{\bar{\mu}_1}{\Sigma_1}\right\|^2 + \Sigma_2\left\|\frac{\bar{\mu}_2}{\Sigma_2}\right\|^2 + \Sigma_3\left\|\frac{\bar{\mu}_3}{\Sigma_3}\right\|^2\right)}_{IV}. \tag{2.25}$$

Since Σ_i may not be always positive, to prove the energy is dissipative, we have to show that two statements hold, (i) $E(\mathbf{u}, \phi_1, \phi_2, \phi_3)$ is always bounded from below; (ii) the term IV in (2.25) is always positive.

If (2.20) is satisfied, from (2.16), we derive $\nabla(\phi_1+\phi_2+\phi_3) = 0$. This implies

$$\sum_{i=1}^{3}\Sigma_i\|\nabla\phi_i\|^2 \geq \underline{\Sigma}\sum_{i=1}^{3}\|\nabla\phi_i\|^2 \geq 0$$

from (2.19). From Remark 2.3 and (2.16), we know that $F(\phi_1, \phi_2, \phi_3)$ is always bounded from below. Therefore $E(\mathbf{u}, \phi_1, \phi_2, \phi_3)$ given in (2.3) is always bounded from below. From (2.18) and (2.19), when (2.20) holds, the term IV is bounded from below since

$$\Sigma_1\left\|\frac{\bar{\mu}_1}{\Sigma_1}\right\|^2 + \Sigma_2\left\|\frac{\bar{\mu}_2}{\Sigma_2}\right\|^2 + \Sigma_3\left\|\frac{\bar{\mu}_3}{\Sigma_3}\right\|^2 \geq \underline{\Sigma}\left(\left\|\frac{\bar{\mu}_1}{\Sigma_1}\right\|^2 + \left\|\frac{\bar{\mu}_2}{\Sigma_2}\right\|^2 + \left\|\frac{\bar{\mu}_3}{\Sigma_3}\right\|^2\right) \geq 0. \tag{2.26}$$

Thus the total energy of the system (2.8)–(2.11) is dissipative (i.e., $\frac{d}{dt}E(\mathbf{u}, \phi_1, \phi_2, \phi_3) \leq 0$), and (2.25) is the associated energy dissipative law. The wellposedness of the model is an interesting future work which may borrow the existing ideas in [75,76].

Remark 2.4. After taking the inner products with suitable functions to derive the PDE energy law (2.25), we note that the term I (from advection) and term II (from surface tension) are canceled by using integration by parts, i.e.,

$$\int_\Omega\big(\phi_i\nabla\mu_i\cdot\mathbf{u} + \nabla\cdot(\mathbf{u}\phi_i)\mu_i\big)d\boldsymbol{x} = 0, i = 1, 2, 3, \tag{2.27}$$

where the boundary conditions (2.13) for $\mathbf{u}$ are used. Similarly, by applying the divergence-free condition and the boundary condition (2.13) for $\mathbf{u}$, it is easy to see that the term III associated with the advection term is also zero, i.e.,

$$\int_\Omega(\mathbf{u}\cdot\nabla)\mathbf{u}\cdot\mathbf{u}d\boldsymbol{x} = 0. \tag{2.28}$$

(2.27) and (2.28) imply that the terms of advection and surface tensions have no any impacts on the energy law, that is, these two kinds of terms can be viewed to satisfy the "zero-contribution-to-energy" property. This view point can help us to design a fully-decoupled scheme in the next section.

3. Numerical methods

To achieve the goal of obtaining a full decoupling scheme, we need to carry out some equivalent reformulations to the original PDE system (2.8)–(2.11).

3.1. Reformulation to an equivalent system

Inspired by (2.27) and (2.28), we introduce a new nonlocal variable $Q(t)$ and its associated ODE system that read as:

$$\begin{cases} Q_t = \lambda \sum_{i=1}^{3} \int_\Omega (\nabla \cdot (\mathbf{u}(\phi_i - \hat{\phi}_i^0))\mu_i + (\phi_i - \hat{\phi}_i^0)\nabla\mu_i \cdot \mathbf{u}) d\boldsymbol{x} + \int_\Omega (\mathbf{u}\cdot\nabla)\mathbf{u}\cdot\mathbf{u} d\boldsymbol{x}, \\ \nabla\cdot\mathbf{u} = 0, \\ Q|_{t=0} = 1, \mathbf{u}|_{\partial\Omega} = \mathbf{0}, \partial_{\mathbf{n}}\phi_i|_{\partial\Omega} = 0,\ i = 1,2,3, \end{cases} \tag{3.1}$$

where $\hat{\phi}_i^0 = \frac{1}{|\Omega|}\int_\Omega \phi_i^0 d\boldsymbol{x}$.

By utilizing (2.27) and (2.28), we find that the ODE (3.1) is trivial indeed, since it is equivalent to: $Q_t = 0$, $Q|_{(t=0)} = 1$. Hence, the exact solution of (3.1) is $Q(t) = 1$. Using the nonlocal variable $Q(t)$, we modify the system (2.8)–(2.11) to the following form:

$$\begin{cases} \phi_{it} + \underbrace{Q\nabla\cdot(\mathbf{u}(\phi_i - \hat{\phi}_i^0))}_{Q-term} = -M\frac{1}{\Sigma_i}\bar{\mu}_i,\ i = 1,2,3, \\ \mu_i = -\frac{3}{4}\epsilon\Sigma_i\Delta\phi_i + \frac{12}{\epsilon}(f_i + \beta_L),\ i = 1,2,3, \\ \mathbf{u}_t + \underbrace{Q\mathbf{u}\cdot\nabla\mathbf{u}}_{Q-term} - \nu\Delta\mathbf{u} + \nabla p + \underbrace{\lambda Q\sum_{i=1}^{3}(\phi_i - \hat{\phi}_i^0)\nabla\mu_i}_{Q-term} = 0, \\ \nabla\cdot\mathbf{u} = 0, \\ Q_t = \lambda\sum_{i=1}^{3}(\nabla\cdot(\mathbf{u}(\phi_i - \hat{\phi}_i^0)), \mu_i) + \lambda\sum_{i=1}^{3}((\phi_i - \hat{\phi}_i^0)\nabla\mu_i, \mathbf{u}) + ((\mathbf{u}\cdot\nabla)\mathbf{u}, \mathbf{u}), \\ Q|_{t=0} = 1, \mathbf{u}|_{\partial\Omega} = \mathbf{0}, \partial_{\mathbf{n}}\phi_i|_{\partial\Omega} = 0,\ i = 1,2,3. \end{cases} \tag{3.2}$$

The above modifications that have been made to the original system (2.8)–(2.11) to obtain the new system (3.2) include the following steps:

- (i) first, we modify the advective term $\nabla\cdot(\mathbf{u}\phi_i)$ to $\nabla\cdot(\mathbf{u}(\phi_i - \hat{\phi}_i^0))$ since $\nabla\cdot(\mathbf{u}\hat{\phi}_i^0) = \nabla\cdot\mathbf{u} = 0$;
- (ii) second, we modify the surface tension term $\sum_{i=1}^3 \phi_i\nabla\mu_i$ to $\sum_{i=1}^3(\phi_i - \hat{\phi}_i^0)\nabla\mu_i$ since $\hat{\phi}_i^0\nabla\mu_i^0 = \nabla(\hat{\phi}_i^0\mu_i^0)$ can be absorbed into the pressure gradient;
- (iii) third, we combine the original system (2.8)–(2.11) with the new ODE (3.1);
- (iv) fourth, we multiply the advection term and the surface tension term with Q. Since $Q(t) = 1$, based on a simple fact of "$a \times 1 = a$", the modified system (3.2) is equivalent to the original system (2.8)–(2.11).

Second, we introduce another nonlocal variable $U(t)$ such that

$$U(t) = \sqrt{(F(\phi_1, \phi_2, \phi_3), 1) + B}, \tag{3.3}$$

where B is a positive constant that is used to ensure the radicand positive. Note that the existence of B is obvious since $F(\phi_1, \phi_2, \phi_3)$ is always bounded from below from Remark 2.3(ii). Note that this boundedness property is valid under the condition $\phi_1 + \phi_2 + \phi_3 = 1$ which will be shown in Remark 3.1. Then, using the variable U, we rewrite the chemical potential μ_i given in the second equation of (3.2) to the following form:

$$\begin{cases} \mu_i = -\frac{3}{4}\epsilon\Sigma_i\Delta\phi_i + \frac{12}{\epsilon}(H_i + \beta)U,\ i = 1,2,3, \\ U_t = \frac{1}{2}\sum_{i=1}^{3}(H_i, \phi_{it}), \\ U|_{(t=0)} = U^0 = \sqrt{(F(\phi_1^0, \phi_2^0, \phi_3^0), 1) + B}, \end{cases} \tag{3.4}$$

where

$$\beta = -\frac{1}{\Sigma_T}\left(\frac{H_1}{\Sigma_1}+\frac{H_2}{\Sigma_2}+\frac{H_3}{\Sigma_3}\right), \tag{3.5}$$

$$H_i = \frac{f_i}{\sqrt{(F(\phi_1,\phi_2,\phi_3),1)+B}}, i = 1,2,3. \tag{3.6}$$

By integrating the second equation in (3.4) and applying the initial condition for $U|_{(t=0)}$, we can obtain the second equation of (3.2). This implies (3.4) is equivalent to the original formulation for μ_i given in (3.2).

Finally, by replacing second equation in (3.2) using (3.4), we obtain a new system that reads as

$$\phi_{it} + Q\nabla\cdot(\mathbf{u}(\phi_i-\hat{\phi}_i^0)) = -M\frac{1}{\Sigma_i}\bar{\mu}_i,\ i=1,2,3, \tag{3.7}$$

$$\mu_i = -\frac{3}{4}\epsilon\Sigma_i\Delta\phi_i + \frac{12}{\epsilon}(H_i+\beta)U,\ i=1,2,3, \tag{3.8}$$

$$U_t = \frac{1}{2}\sum_{i=1}^{3}(H_i,\phi_{it}), \tag{3.9}$$

$$\mathbf{u}_t + Q\mathbf{u}\cdot\nabla\mathbf{u} - \nu\Delta\mathbf{u} + \nabla p + \lambda Q\sum_{i=1}^{3}(\phi_i-\hat{\phi}_i^0)\nabla\mu_i = 0, \tag{3.10}$$

$$\nabla\cdot\mathbf{u} = 0, \tag{3.11}$$

$$Q_t = \lambda\sum_{i=1}^{3}(\nabla\cdot(\mathbf{u}(\phi_i-\hat{\phi}_i^0)),\mu_i) + \lambda\sum_{i=1}^{3}((\phi_i-\hat{\phi}_i^0)\nabla\mu_i,\mathbf{u}) + ((\mathbf{u}\cdot\nabla)\mathbf{u},\mathbf{u}), \tag{3.12}$$

with the initial conditions that read as

$$\begin{cases}\mathbf{u}|_{(t=0)} = \mathbf{u}^0,\ p|_{(t=0)} = p^0,\ Q|_{(t=0)} = 1, U|_{(t=0)} = U^0,\\ \phi_1|_{(t=0)} = \phi_1^0, \phi_2|_{(t=0)} = \phi_2^0, \phi_3|_{(t=0)} = \phi_3^0, \phi_1^0+\phi_2^0+\phi_3^0 = 1,\end{cases} \tag{3.13}$$

and the boundary conditions that read as

$$\mathbf{u}|_{\partial\Omega} = \mathbf{0},\ \partial_{\mathbf{n}}\phi_i|_{\partial\Omega} = 0,\ i=1,2,3. \tag{3.14}$$

Remark 3.1. Eqs. (3.7)–(3.8) are equivalent to the following two phase-field variables system

$$\begin{cases}\phi_{it} + Q\nabla\cdot(\mathbf{u}(\phi-\hat{\phi}_i^0)) = -M\frac{1}{\Sigma_i}\bar{\mu}_i,\ i=1,2,\\ \mu_i = -\frac{3}{4}\epsilon\Sigma_i\Delta\phi_i + \frac{12}{\epsilon}(H_i+\beta)U,\ i=1,2,\end{cases} \tag{3.15}$$

and ϕ_3, μ_3, $\bar{\mu}_3$ are given by the following explicit formula:

$$\phi_1+\phi_2+\phi_3 = 1, \tag{3.16}$$

$$\frac{\mu_1}{\Sigma_1}+\frac{\mu_2}{\Sigma_2}+\frac{\mu_3}{\Sigma_3} = 0, \tag{3.17}$$

$$\frac{\bar{\mu}_1}{\Sigma_1}+\frac{\bar{\mu}_2}{\Sigma_2}+\frac{\bar{\mu}_3}{\Sigma_3} = 0. \tag{3.18}$$

Since the proof is quite similar to Theorem 3.1, we omit the details here.

From the above-detailed reformulations, it is easy to see the new system (3.7)–(3.12) with the initial conditions (3.13) and boundary conditions (3.14) is equivalent to the original system (2.8)–(2.13). Thus, the new system (3.7)–(3.14) also holds the energy dissipation law by performing a similar process to obtain (2.25). Since the energy stability proof at the discrete level follows the same line, we perform the detailed derivation for comparisons.

We multiply the L^2 inner product of (3.7) with $\lambda\mu_i$ and take the summation for $i = 1, 2, 3$ to get

$$\lambda\sum_{i=1}^{3}(\phi_{it},\mu_i) = -M\lambda\sum_{i=1}^{3}\Sigma_i\left\|\frac{\bar{\mu}_i}{\Sigma_i}\right\|^2 \underbrace{-\lambda Q\sum_{i=1}^{3}(\nabla\cdot(\mathbf{u}(\phi_i-\hat{\phi}_i^0)),\mu_i)}_{\mathrm{I}_1}. \tag{3.19}$$

We multiply the L^2 inner product of (3.8) with $-\lambda\phi_{it}$ and take the summation for $i = 1, 2, 3$ to get

$$-\lambda\sum_{i=1}^{3}(\mu_i,\phi_{it}) + \lambda\frac{3}{8}\epsilon\frac{d}{dt}\left(\sum_{i=1}^{3}\Sigma_i\|\nabla\phi_i\|^2\right) = \underbrace{-\lambda\frac{12}{\epsilon}\sum_{i=1}^{3}U(H_i,\phi_{it})}_{\mathrm{IV}_1} - \lambda\frac{12}{\epsilon}(\beta,\sum_{i=1}^{3}\phi_{it}). \tag{3.20}$$

We multiply (3.9) with $\lambda\frac{24}{\epsilon}U$ to derive

$$\frac{d}{dt}\left(\lambda\frac{12}{\epsilon}|U|^2\right) = \underbrace{\lambda\frac{12}{\epsilon}\sum_{i=1}^{3}U(H_i,\phi_{it})}_{\mathrm{IV}_2}. \tag{3.21}$$

By multiplying the L^2 inner product of (3.10) with $\mathbf{u}$, we get

$$\frac{1}{2}\frac{d}{dt}\|\mathbf{u}\|^2 + \nu\|\nabla\mathbf{u}\|^2 - (p,\nabla\cdot\mathbf{u}) = \underbrace{-\lambda Q\sum_{i=1}^{3}((\phi_i-\hat{\phi}_i^0)\nabla\mu_i,\mathbf{u})}_{\mathrm{II}_1}\underbrace{-Q((\mathbf{u}\cdot\nabla)\mathbf{u},\mathbf{u})}_{\mathrm{III}_1}. \tag{3.22}$$

By multiplying (3.12) with Q, we get

$$\frac{d}{dt}\left(\frac{1}{2}|Q|^2\right) = \underbrace{\lambda Q\sum_{i=1}^{3}(\nabla\cdot(\mathbf{u}(\phi_i-\hat{\phi}_i^0)),\mu_i)}_{\mathrm{I}_2} + \underbrace{\lambda Q\sum_{i=1}^{3}((\phi_i-\hat{\phi}_i^0)\nabla\mu_i,\mathbf{u})}_{\mathrm{II}_2} + \underbrace{Q((\mathbf{u}\cdot\nabla\mathbf{u}),\mathbf{u})}_{\mathrm{III}_2}. \tag{3.23}$$

Combining the above five equalities (3.19)–(3.23), using $(\beta,\sum_{i=1}^{3}\phi_{it}) = (\beta,(1)_t) = 0$, noting that the two terms with the same Roman numerals under curly braces cancel each other out, and using (3.16) and (3.18), we derive

$$\begin{aligned}\frac{d}{dt}E(\mathbf{u},\phi_1,\phi_2,\phi_3,U,Q) &= -\nu\|\nabla\mathbf{u}\|^2 - \lambda M\left(\Sigma_1\left\|\frac{\bar{\mu}_1}{\Sigma_1}\right\|^2 + \Sigma_2\left\|\frac{\bar{\mu}_2}{\Sigma_2}\right\|^2 + \Sigma_3\left\|\frac{\bar{\mu}_3}{\Sigma_3}\right\|^2\right)\\ &\le -\nu\|\nabla\mathbf{u}\|^2 - \lambda M\underline{\Sigma}\left(\left\|\frac{\bar{\mu}_1}{\Sigma_1}\right\|^2 + \left\|\frac{\bar{\mu}_2}{\Sigma_2}\right\|^2 + \left\|\frac{\bar{\mu}_3}{\Sigma_3}\right\|^2\right) \le 0,\end{aligned} \tag{3.24}$$

where

$$E(\mathbf{u},\phi_1,\phi_2,\phi_3,U,Q) = \frac{1}{2}\|\mathbf{u}\|^2 + \lambda\frac{3}{8}\epsilon\sum_{i=1}^{3}\Sigma_i\|\nabla\phi_i\|^2 + \lambda\frac{12}{\epsilon}|U|^2 + \frac{1}{2}|Q|^2, \tag{3.25}$$

that is bounded from below from (2.19).

Remark 3.2. After taking the inner products of the suitable functions to derive the energy law for the original PDE system (2.8)–(2.11), we notice that the terms associated with the advection (term I in (2.21)) and surface tension term (term III in (2.24)) cancel each other out, this means the discretization of these two terms must be matched, thereby leading to the coupled type schemes.

But for the newly modified system (3.7)–(3.14), from the derivation of the energy law, it can be seen that we no longer require that the discretization of these two terms must match, because the ODE (3.12) could provide all needed terms that can cancel all trouble terms (e.g., I_1 in (3.19) can be canceled by I_2 in (3.23) instead of II_1 in (3.22))). In other words, when developing numerical schemes, we can use different discretization methods to deal with the advection term I_1 and surface tension term II_1, so that it is possible to construct a full decoupling type

scheme. This technique using the auxiliary variable Q to handle the coupling terms of surface tension and advection is motivated from the SAV method [6,7,77] that can only handle a single system. This article innovatively applies the method of auxiliary variables to deal with coupling systems.

3.2. Numerical scheme

In this subsection, we develop a fully-discrete numerical algorithm for the system (3.7)–(3.12), which is an equivalent system of the hydrodynamically-coupled ternary model (2.8)–(2.11).

Some finite-dimensional discrete subspaces are introduced here. Suppose that the polygonal/polyhedral domain Ω is discretized by a conforming and shape regular triangulation/tetrahedron mesh $\mathcal{T}_h$ that is composed by open disjoint elements K such that $\bar{\Omega} = \bigcup_{K\in\mathcal{T}_h} \bar{K}$. We use $\mathcal{P}_l$ to denote the space of polynomials of total degree at most l and define the following finite element spaces:

$$\begin{aligned} Y_h &= \left\{\phi \in C^0(\Omega) : \phi|_K \in \mathcal{P}_{l_1}(K), \forall K \in \mathcal{T}_h\right\}, \\ \boldsymbol{V}_h &= \left\{\boldsymbol{v} \in C^0(\Omega)^d : \boldsymbol{v}|_K \in \mathcal{P}_{l_2}(K)^d, \forall K \in \mathcal{T}_h\right\} \cap H_0^1(\Omega)^d, \\ O_h &= \left\{q \in C^0(\Omega) : q|_K \in \mathcal{P}_{l_2-1}(K), \forall K \in \mathcal{T}_h\right\} \cap L_0^2(\Omega), \end{aligned} \tag{3.26}$$

where $H_0^1(\Omega) = \{u \in H^1(\Omega) : u|_{\partial\Omega} = 0\}$ and $L_0^2(\Omega) = \{q \in L^2(\Omega) : \int_\Omega q dx = 0\}$. Hence,

$$Y_h \subset H^1(\Omega),\ \boldsymbol{V}_h \subset H_0^1(\Omega)^d,\ O_h \subset L_0^2(\Omega). \tag{3.27}$$

Besides, we assume the pair of spaces $(\boldsymbol{V}_h, O_h)$ satisfy the *inf–sup* condition [78]:

$$\beta_c \|q\| \le \sup_{\boldsymbol{v}\in\boldsymbol{V}_h} \frac{(\nabla\cdot\boldsymbol{v}, q)}{\|\nabla\boldsymbol{v}\|}, \quad \forall q \in O_h,$$

where the constant β_c only depends on Ω. A well known *inf–sup* stable pair $(\boldsymbol{V}_h, O_h)$ is the Taylor–Hood element [78].

The semi-discrete formulations of the system (3.7)–(3.12) in the weak form reads as: find $\phi_i,\ \mu_i \in H^1(\Omega)$, $Q, U \in \mathbb{R}$, $\mathbf{u} \in H_0^1(\Omega)^d$, $p \in L_0^2(\Omega)$, such that

$$(\phi_{it}, w) - Q(\mathbf{u}(\phi_i - \hat{\phi}_i^0), \nabla w) = -M\frac{1}{\Sigma_i}(\bar{\mu}_i, w), i = 1, 2, 3, \tag{3.28}$$

$$(\mu_i, \Theta) = \frac{3}{4}\epsilon\Sigma_i(\nabla\phi_i, \nabla\Theta) + \frac{12}{\epsilon}U(H_i + \beta, \Theta), i = 1, 2, 3, \tag{3.29}$$

$$U_t = \frac{1}{2}\sum_{i=1}^{3}(H_i, \phi_{it}), \tag{3.30}$$

$$(\mathbf{u}_t, \mathbf{v}) + Q((\mathbf{u}\cdot\nabla)\mathbf{u}, \mathbf{v}) + \nu(\nabla\mathbf{u}, \nabla\mathbf{v}) - (p, \nabla\cdot\mathbf{v}) + Q\sum_{i=1}^{3}((\phi_i - \hat{\phi}_i^0)\nabla\mu_i, \mathbf{v}) = 0, \tag{3.31}$$

$$(\nabla\cdot\mathbf{u}, q) = 0, \tag{3.32}$$

$$Q_t = -\lambda\sum_{i=1}^{3}(\mathbf{u}(\phi_i - \hat{\phi}_i^0), \nabla\mu_i) + \lambda\sum_{i=1}^{3}((\phi_i - \hat{\phi}_i^0)\nabla\mu_i, \mathbf{u}) + ((\mathbf{u}\cdot\nabla)\mathbf{u}, \mathbf{u}), \tag{3.33}$$

for $\Theta, w \in H^1(\Omega)$, $\mathbf{v} \in H_0^1(\Omega)^d$, $q \in L_0^2(\Omega)$.

We let $\delta t > 0$ be a time step size and $t^n = n\delta t$ for $0 \le n \le N$ with $T = N\delta t$, and use ψ_h^n to denote the numerical approximation in the related finite element space to the function $\psi(\cdot, t)$ at $t = t^n$. For the weak form (3.28)–(3.33), we construct a time marching scheme based on the second-order backward differentiation formula (BDF2) as follows.

Find $\phi_{ih}^{n+1},\ \mu_{ih}^{n+1} \in Y_h$, $U^{n+1}, Q^{n+1} \in \mathbb{R}$, $\tilde{\mathbf{u}}_h^{n+1} \in \boldsymbol{V}_h$, $p_h^{n+1} \in O_h$, such that

$$\begin{aligned} &(\frac{a\tilde{\mathbf{u}}_h^{n+1} - b\mathbf{u}_h^n + c\mathbf{u}_h^{n-1}}{2\delta t}, \mathbf{v}_h) + Q^{n+1}((\mathbf{u}^*\cdot\nabla)\mathbf{u}^*, \mathbf{v}_h) + \nu(\nabla\tilde{\mathbf{u}}_h^{n+1}, \nabla\mathbf{v}_h) \\ &\qquad + (\nabla p_h^n, \mathbf{v}_h) + \lambda Q^{n+1}\sum_{i=1}^{3}((\phi_i^* - \hat{\phi}_i^0)\nabla\mu_i^*, \mathbf{v}_h) = 0, \end{aligned} \tag{3.34}$$

$$(\frac{a\phi_{ih}^{n+1}-b\phi_{ih}^{n}+c\phi_{ih}^{n-1}}{2\delta t}, w_h) - Q^{n+1}(\mathbf{u}^*(\phi_i^*-\hat{\phi}_i^0), \nabla w_h) = -M\frac{1}{\Sigma_i}(\bar{\mu}_{ih}^{n+1}, w_h), i=1,2,3, \tag{3.35}$$

$$(\mu_{ih}^{n+1}, \Theta_h) = \frac{3}{4}\epsilon\Sigma_i(\nabla\phi_{ih}^{n+1}, \nabla\Theta_h) + \frac{12}{\epsilon}(H_i^*+\beta^*, \Theta_h)U^{n+1} + \frac{S}{\epsilon}\Sigma_i((\phi_{ih}^{n+1}-\phi_{ih}^*), \Theta_h), i=1,2,3, \tag{3.36}$$

$$aU^{n+1}-bU^n+cU^{n-1} = \frac{1}{2}\sum_{i=1}^{3}(H_i^*, a\phi_{ih}^{n+1}-b\phi_{ih}^n+c\phi_{ih}^{n-1}), \tag{3.37}$$

$$\frac{1}{2\delta t}(aQ^{n+1}-bQ^n+cQ^{n-1}) = -\lambda\sum_{i=1}^{3}(\mathbf{u}^*(\phi_i^*-\hat{\phi}_i^0), \nabla\mu_{ih}^{n+1}) + \lambda\sum_{i=1}^{3}((\phi_i^*-\hat{\phi}_i^0)\nabla\mu_i^*, \tilde{\mathbf{u}}_h^{n+1}) + ((\mathbf{u}^*\cdot\nabla)\mathbf{u}^*\cdot\tilde{\mathbf{u}}_h^{n+1}), \tag{3.38}$$

$$(\nabla(p_h^{n+1}-p_h^n), \nabla q_h) = -\frac{2}{\delta t}(\nabla\cdot\tilde{\mathbf{u}}_h^{n+1}, q_h), \tag{3.39}$$

$$\mathbf{u}_h^{n+1} = \tilde{\mathbf{u}}_h^{n+1} - \frac{\delta t}{2}(\nabla p_h^{n+1}-\nabla p_h^n), \tag{3.40}$$

where

$$\begin{cases} a=3, b=4, c=1,\ \mathbf{u}^*=2\mathbf{u}_h^n-\mathbf{u}_h^{n-1}, \phi_i^*=2\phi_{ih}^n-\phi_{ih}^{n-1}, \\ \mu_i^*=2\mu_{ih}^n-\mu_{ih}^{n-1}, H_i^*=H_i(\phi_1^*,\phi_2^*,\phi_3^*), \beta^*=-\dfrac{1}{\Sigma_T}\left(\dfrac{H_1^*}{\Sigma_1}+\dfrac{H_2^*}{\Sigma_2}+\dfrac{H_3^*}{\Sigma_3}\right), \end{cases} \tag{3.41}$$

$S>0$ is a stabilization parameter. Some detailed explanations of the scheme are given in the following remarks.

Remark 3.3. From the discretization method of (3.38), it can be seen that the discrete value of Q^{n+1} will not be strictly equal to 1, because the integral terms in (3.38) are not equal to zero. This is completely reasonable since Q^{n+1} is only a numerical approximation to the exact solution $Q(t)|_{t^{n+1}}=1$. That is, Q^{n+1} will approximate to $Q(t)$ with a certain order of accuracy.

Remark 3.4. For the Navier–Stokes equation, the second-order pressure-correction scheme is used to decouple the computation of the pressure from that of the velocity. We refer to [9] for an extensive overview of projection-type methods. This projection method was analyzed in [79], where it is shown (discrete in time, continuous in space) that the scheme is second-order accurate for velocity but only first-order accurate for pressure. The loss of pressure accuracy is caused by the artificial Neumann boundary condition imposed on the pressure [80]. The final solution $\mathbf{u}_h^{n+1}$ satisfies the discrete divergence-free condition, which can be deduced by taking the L^2 inner product of (3.40) with $\nabla q_h \in O_h$, that is

$$(\mathbf{u}_h^{n+1}, \nabla q_h) = (\tilde{\mathbf{u}}_h^{n+1}, \nabla q_h) - \frac{\delta t}{2}(\nabla(p_h^{n+1}-p_h^n), \nabla q_h). \tag{3.42}$$

From the boundary condition of $\tilde{\mathbf{u}}_h^{n+1}$, we derive $(\tilde{\mathbf{u}}_h^{n+1}, \nabla q_h) = -(\nabla\cdot\tilde{\mathbf{u}}_h^{n+1}, q_h)$ by applying integration by parts. Therefore, from (3.39), we derive

$$(\mathbf{u}_h^{n+1}, \nabla q_h) = 0. \tag{3.43}$$

Remark 3.5. The initialization of the second-order scheme requires all values at $t=t^1$, which can be obtained by constructing the first-order scheme based on the backward Euler method. By setting $a=2, b=2, c=0, \psi^*=\psi^0$ for any variable ψ, the first-order scheme can be easily obtained. Moreover, by using mathematical induction, it is easy to conclude that the following volume conservation property holds:

$$\int_\Omega \phi_{ih}^{n+1}d\boldsymbol{x} = \int_\Omega \phi_{ih}^n d\boldsymbol{x} = \cdots = \int_\Omega \phi_{ih}^0 d\boldsymbol{x},\ i=1,2,3. \tag{3.44}$$

Remark 3.6. When the system has very high stiffness issues caused by the model parameters or other conditions, exceedingly small time steps are needed to achieve reasonable accuracy while some numerical methods are formally unconditionally energy stable, see the stabilized-IEQ/SAV methods in [7,77,81–84]. To fix such an inherent deficiency, a commonly used effective way is to add an extra linear stabilization term with the corresponding temporal order (cf. the second-order term related to S in (3.36)). The scale of the splitting errors caused by this term is about $\sim \frac{S}{\epsilon^2}\delta t^2 \partial_{tt}\phi(\cdot)$, which is actually consistent with the error caused by the second-order extrapolated nonlinear term $f(\phi)$. In Section 4, we present numerical evidence to show that this stabilizer is effective to improve the energy stability while using large time steps in Fig. 4.2. Similar linear stabilization techniques had been widely used in the numerical scheme for solving the phase-field type models, e.g., the methods of linear stabilization, IEQ, SAV, convex-splitting methods, etc., see [5,7,77,81–89].

The following theorem ensures the numerical solutions $\phi_{1h}^{n+1}, \phi_{2h}^{n+1}, \phi_{3h}^{n+1}$ computed by the scheme (3.34)–(3.40) always satisfy the free-leakage condition $\sum_{i=1}^{3}\phi_{ih}^{n+1}=1$, namely, no volume loss.

Theorem 3.1. *The system (3.35)–(3.36) with three phase-field variables is equivalent to the following scheme involving the computations of two unknown phase-field variables,*

$$(\frac{3\phi_{ih}^{n+1}-4\phi_{ih}^{n}+\phi_{ih}^{n-1}}{2\delta t}, w_h) - Q^{n+1}(\mathbf{u}^*(\phi_i^*-\hat{\phi}_i^0), \nabla w_h) = -M\frac{1}{\Sigma_i}(\bar{\mu}_{ih}^{n+1}, w_h), i=1,2, \tag{3.45}$$

$$(\mu_{ih}^{n+1}, \Theta_h) = \frac{3}{4}\epsilon\Sigma_i(\nabla\phi_{ih}^{n+1}, \nabla\Theta_h) + \frac{12}{\epsilon}(H_i^*+\beta^*, \Theta_h)U^{n+1} + \frac{S}{\epsilon}\Sigma_i(\phi_{ih}^{n+1}-\phi_{ih}^*, \Theta_h), i=1,2. \tag{3.46}$$

The variables $\phi_{3h}^{n+1}, \mu_{3h}^{n+1}, \bar{\mu}_{3h}^{n+1}$ can be updated by the following relations:

$$\phi_{3h}^{n+1} = 1-\phi_{1h}^{n+1}-\phi_{2h}^{n+1}, \tag{3.47}$$

$$\frac{\mu_{3h}^{n+1}}{\Sigma_3} = -(\frac{\mu_{1h}^{n+1}}{\Sigma_1}+\frac{\mu_{2h}^{n+1}}{\Sigma_2}), \tag{3.48}$$

$$\frac{\bar{\mu}_{3h}^{n+1}}{\Sigma_3} = -(\frac{\bar{\mu}_{1h}^{n+1}}{\Sigma_1}+\frac{\bar{\mu}_{2h}^{n+1}}{\Sigma_2}). \tag{3.49}$$

Proof. First, we derive (3.35)–(3.36) by assuming (3.45)–(3.49) are satisfied. We take the sum of (3.45) for $i=1,2$ to obtain

$$(\frac{3\phi_{3h}^{n+1}-4\phi_{3h}^{n}+\phi_{3h}^{n-1}}{2\delta t}, w_h) - Q^{n+1}(\mathbf{u}^*(\phi_3^*-\hat{\phi}_3^0), \nabla w_h) = -M\frac{1}{\Sigma_3}(\bar{\mu}_{3h}^{n+1}, w_h), \tag{3.50}$$

where we use (3.47) at $t=t^{n+1}, t^n, t^{n-1}$, (3.49), and (3.43).

Furthermore, from (3.47), (3.48), and the definition of β^* in (3.41), we derive

$$\begin{aligned}(\mu_{3h}^{n+1}, \Theta_h) &= -\Sigma_3(\frac{\mu_{1h}^{n+1}}{\Sigma_1}+\frac{\mu_{2h}^{n+1}}{\Sigma_2}, \Theta_h)\\ &= -\Sigma_3\Big(\frac{3}{4}\epsilon(\nabla(\phi_{1h}^{n+1}+\phi_{2h}^{n+1}), \nabla\Theta_h) + \frac{12}{\epsilon}\Big(\frac{H_1^*+\beta^*}{\Sigma_1}+\frac{H_2^*+\beta^*}{\Sigma_2}, \Theta_h\Big)U^{n+1}\\ &\qquad + \frac{S}{\epsilon}(\phi_{1h}^{n+1}+\phi_{2h}^{n+1}-\phi_1^*-\phi_2^*, \Theta_h)\Big)\\ &= \frac{3}{4}\epsilon\Sigma_3(\nabla\phi_{3h}^{n+1}, \nabla\Theta_h) + \frac{12}{\epsilon}(H_3^*+\beta^*, \Theta_h)U^{n+1} + \frac{S}{\epsilon}\Sigma_3(\phi_{3h}^{n+1}-\phi_3^*, \Theta_h).\end{aligned}$$

where we use the identity

$$\frac{H_1^*+\beta^*}{\Sigma_1}+\frac{H_2^*+\beta^*}{\Sigma_2}+\frac{H_3^*+\beta^*}{\Sigma_3}=0, \tag{3.51}$$

that is the reformulation of (3.41).

Second, we assume that Eqs. (3.35)–(3.36) are satisfied and derive (3.45)–(3.49). We use mathematical induction and assume (3.47) are valid for $t=t^n$ and $t=t^{n-1}$. The validity of (3.47) at $t=t^1$ can be shown by taking a similar procedure of proof for the first-order version of the scheme, see Remark 3.5.

For any m, we define

$$\Phi^m = \phi_{1h}^m + \phi_{2h}^m + \phi_{3h}^m,\ \mu^m = \frac{\mu_{1h}^m}{\Sigma_1} + \frac{\mu_{2h}^m}{\Sigma_2} + \frac{\mu_{3h}^m}{\Sigma_3}. \tag{3.52}$$

By taking the summation of (3.35) for $i = 1, 2, 3$, we derive

$$\frac{3}{2\delta t}(\Phi^{n+1} - 1, w_h) = -M(\bar{\mu}^{n+1}, w_h), \tag{3.53}$$

where the combination of three advective terms vanishes that is because

$$\begin{aligned} Q^{n+1}\sum_{i=1}^{3}(\mathbf{u}^*(\phi_i^* - \hat{\phi}_i^0), \nabla w_h) &= Q^{n+1}(\mathbf{u}^*\sum_{i=1}^{3}(\phi_i^* - \hat{\phi}_i^0), \nabla w_h) \\ &= Q^{n+1}(\mathbf{u}^*(1-1), \nabla w_h) = 0. \end{aligned} \tag{3.54}$$

By taking the summation of (3.36) for $i = 1, 2, 3$, and using the identity (3.51), we derive

$$(\mu^{n+1}, \Theta_h) = \frac{3}{4}\epsilon(\nabla\Phi^{n+1}, \nabla\Theta_h) + \frac{S}{\epsilon}(\Phi^{n+1} - 1, \Theta_h). \tag{3.55}$$

Taking $w_h = -\frac{2\delta t}{3}\mu^{n+1}$ in (3.53), and $\Theta_h = \Phi^{n+1} - 1$ in (3.55), and taking the summation of the two obtained equations, we derive

$$\frac{3}{4}\epsilon\|\nabla\Phi^{n+1}\|^2 + \frac{S}{\epsilon}\|\Phi^{n+1} - 1\|^2 + \frac{2\delta t}{3}M\|\bar{\mu}^{n+1}\|^2 = 0. \tag{3.56}$$

Since the left hand side of (3.56) is a sum of non-negative terms, thus $\bar{\mu}^{n+1} = 0$ and $\Phi^{n+1} = 1$, i.e., (3.47) is valid. Hence, from (3.55), we get $\mu^{n+1} = 0$ that implies (3.48) and (3.49). □

3.3. Implementation

In this subsection, we discuss how to obtain the decoupled structure of the scheme (3.34)–(3.40), where we make full use of the nonlocal features of the two additional variables U and Q.

Step 1. First, we use the nonlocal scalar variable Q^{n+1} to split $\phi_{ih}^{n+1}, \mu_{ih}^{n+1}, U^{n+1}$ for $i = 1, 2, 3$ into a linear combination form that reads as

$$\begin{cases} \phi_{ih}^{n+1} = \phi_{i1h}^{n+1} + Q^{n+1}\phi_{i2h}^{n+1}, \mu_{ih}^{n+1} = \mu_{i1h}^{n+1} + Q^{n+1}\mu_{i2h}^{n+1}, \\ \bar{\mu}_{ih}^{n+1} = \bar{\mu}_{i1h}^{n+1} + Q^{n+1}\bar{\mu}_{i2h}^{n+1}, U^{n+1} = U_1^{n+1} + Q^{n+1}U_2^{n+1}. \end{cases} \tag{3.57}$$

Then the scheme (3.35)–(3.36) can be rewritten as

$$\begin{cases} \frac{a}{2\delta t}(\phi_{i1h}^{n+1} + Q^{n+1}\phi_{i2h}^{n+1}, w_h) - Q^{n+1}(\mathbf{u}^*(\phi_i^* - \hat{\phi}_i^0), \nabla w_h) \\ \qquad = -M\frac{1}{\Sigma_i}\left(\bar{\mu}_{i1h}^{n+1} + Q^{n+1}\bar{\mu}_{i2h}^{n+1}, w_h\right) + (\frac{b\phi_{ih}^n - c\phi_{ih}^{n-1}}{2\delta t}, w_h), \\ (\mu_{i1h}^{n+1} + Q^{n+1}\mu_{i2h}^{n+1}, \Theta_h) = \frac{3}{4}\epsilon\Sigma_i(\nabla(\phi_{i1h}^{n+1} + Q^{n+1}\phi_{i2h}^{n+1}), \nabla\Theta_h) \\ \qquad + \frac{12}{\epsilon}(H_i^* + \beta^*, \Theta_h)(U_1^{n+1} + Q^{n+1}U_2^{n+1}) \\ \qquad + \frac{S}{\epsilon}\Sigma_i(\phi_{i1h}^{n+1} + Q^{n+1}\phi_{i2h}^{n+1} - \phi_i^*, \Theta_h). \end{cases} \tag{3.58}$$

According to Q^{n+1}, we split the system (3.58) into two sub-systems as follows,

$$\begin{cases} \frac{a}{2\delta t}(\phi_{i1h}^{n+1}, w_h) = -M\frac{1}{\Sigma_i}(\bar{\mu}_{i1h}^{n+1}, w_h) + (\frac{b\phi_{ih}^n - c\phi_{ih}^{n-1}}{2\delta t}, w_h), \\ (\mu_{i1h}^{n+1}, \Theta_h) = \frac{3}{4}\epsilon\Sigma_i(\nabla\phi_{i1h}^{n+1}, \nabla\Theta_h) + \frac{12}{\epsilon}(H_i^* + \beta^*, \Theta_h)U_1^{n+1} + \frac{S}{\epsilon}\Sigma_i(\phi_{i1h}^{n+1} - \phi_i^*, \Theta_h), \end{cases} \tag{3.59}$$

$$\begin{cases} \dfrac{a}{2\delta t}(\phi_{i2h}^{n+1}, w_h) = -M\dfrac{1}{\Sigma_i}(\bar{\mu}_{i2h}^{n+1}, w_h) + (\mathbf{u}^*(\phi_i^* - \hat{\phi}_i^0), \nabla w_h), \\ (\mu_{i2h}^{n+1}, \Theta_h) = \dfrac{3}{4}\epsilon\Sigma_i(\nabla\phi_{i2h}^{n+1}, \nabla\Theta_h) + \dfrac{12}{\epsilon}(H_i^* + \beta^*, \Theta_h)U_2^{n+1} + \dfrac{S}{\epsilon}\Sigma_i(\phi_{i2h}^{n+1}, \Theta_h). \end{cases} \tag{3.60}$$

By applying a procedure similar to the second step of the proof in Theorem 3.1 to the two sub-systems (3.59) and (3.60), we derive

$$\begin{cases} \phi_{11h}^{n+1} + \phi_{21h}^{n+1} + \phi_{31h}^{n+1} = 1, \ \dfrac{\mu_{11h}^{n+1}}{\Sigma_i} + \dfrac{\mu_{21h}^{n+1}}{\Sigma_2} + \dfrac{\mu_{31h}^{n+1}}{\Sigma_3} = 0, \ \dfrac{\bar{\mu}_{11h}^{n+1}}{\Sigma_i} + \dfrac{\bar{\mu}_{21h}^{n+1}}{\Sigma_2} + \dfrac{\bar{\mu}_{31h}^{n+1}}{\Sigma_3} = 0, \\ \phi_{12h}^{n+1} + \phi_{22h}^{n+1} + \phi_{32h}^{n+1} = 0, \ \dfrac{\mu_{12h}^{n+1}}{\Sigma_i} + \dfrac{\mu_{22h}^{n+1}}{\Sigma_2} + \dfrac{\mu_{32h}^{n+1}}{\Sigma_3} = 0, \ \dfrac{\bar{\mu}_{12h}^{n+1}}{\Sigma_i} + \dfrac{\bar{\mu}_{22h}^{n+1}}{\Sigma_2} + \dfrac{\bar{\mu}_{32h}^{n+1}}{\Sigma_3} = 0. \end{cases} \tag{3.61}$$

Moreover, by setting $w_h = 1$ in (3.59) and (3.60), we obtain

$$\int_\Omega \phi_{i1h}^{n+1} d\boldsymbol{x} = \int_\Omega \phi_{ih}^{n} d\boldsymbol{x} = \cdots = \int_\Omega \phi_{ih}^{0} d\boldsymbol{x}, \ \int_\Omega \phi_{i2h}^{n+1} d\boldsymbol{x} = 0, i = 1, 2, 3. \tag{3.62}$$

We continue to use the splitting technique for the variables $\phi_{i1h}^{n+1}, \mu_{i1h}^{n+1}, i = 1, 2, 3$, namely, they are split into a linear combination form by using two nonlocal variables U_1^{n+1} and U_2^{n+1}, which reads as

$$\begin{cases} \phi_{i1h}^{n+1} = \phi_{i11h}^{n+1} + U_1^{n+1}\phi_{i12h}^{n+1}, & \mu_{i1h}^{n+1} = \mu_{i11h}^{n+1} + U_1^{n+1}\mu_{i12h}^{n+1}, \\ \phi_{i2h}^{n+1} = \phi_{i21h}^{n+1} + U_2^{n+1}\phi_{i22h}^{n+1}, & \mu_{i2h}^{n+1} = \mu_{i21h}^{n+1} + U_2^{n+1}\mu_{i22h}^{n+1}. \end{cases} \tag{3.63}$$

By substituting the split form of all variables in (3.63) into (3.59)–(3.60), and decomposing the results according to the nonlocal variable U_1^{n+1} and U_2^{n+1}, we obtain the following four independent subsystems that read as

$$\begin{cases} \dfrac{a}{2\delta t}(\phi_{i11h}^{n+1}, w_h) = -M\dfrac{1}{\Sigma_i}(\bar{\mu}_{i11h}^{n+1}, w_h) + (\dfrac{b\phi_{ih}^{n} - c\phi_{ih}^{n-1}}{2\delta t}, w_h), \\ (\mu_{i11h}^{n+1}, \Theta_h) = \dfrac{3}{4}\epsilon\Sigma_i(\nabla\phi_{i11h}^{n+1}, \nabla\Theta_h) + \dfrac{S}{\epsilon}\Sigma_i(\phi_{i11h}^{n+1} - \phi_i^*, \Theta_h), \end{cases} \tag{3.64}$$

$$\begin{cases} \dfrac{a}{2\delta t}(\phi_{i12h}^{n+1}, w_h) = -M\dfrac{1}{\Sigma_i}(\bar{\mu}_{i12h}^{n+1}, w_h), \\ (\mu_{i12h}^{n+1}, \Theta_h) = \dfrac{3}{4}\epsilon\Sigma_i(\nabla\phi_{i12h}^{n+1}, \nabla\Theta_h) + \dfrac{12}{\epsilon}(H_i^* + \beta^*, \Theta_h) + \dfrac{S}{\epsilon}\Sigma_i(\phi_{i12h}^{n+1}, \Theta_h), \end{cases} \tag{3.65}$$

$$\begin{cases} \dfrac{a}{2\delta t}(\phi_{i21h}^{n+1}, w_h) = -M\dfrac{1}{\Sigma_i}(\bar{\mu}_{i21h}^{n+1}, w_h) + (\mathbf{u}^*(\phi_i^* - \hat{\phi}_i^0), \nabla w_h), \\ (\mu_{i21h}^{n+1}, \Theta_h) = \dfrac{3}{4}\epsilon\Sigma_i(\nabla\phi_{i21h}^{n+1}, \nabla\Theta_h) + \dfrac{S}{\epsilon}\Sigma_i(\phi_{i21h}^{n+1}, \Theta_h), \end{cases} \tag{3.66}$$

$$\begin{cases} \dfrac{a}{2\delta t}(\phi_{i22h}^{n+1}, w_h) = -M\dfrac{1}{\Sigma_i}(\bar{\mu}_{i22h}^{n+1}, w_h), \\ (\mu_{i22h}^{n+1}, \Theta_h) = \dfrac{3}{4}\epsilon\Sigma_i(\nabla\phi_{i22h}^{n+1}, \nabla\Theta_h) + \dfrac{12}{\epsilon}(H_i^* + \beta^*, \Theta_h) + \dfrac{S}{\epsilon}\Sigma_i(\phi_{i22h}^{n+1}, \Theta_h). \end{cases} \tag{3.67}$$

Note that the two sub-systems (3.65) and (3.67) are identical which implies $\phi_{i12h}^{n+1} = \phi_{i22h}^{n+1}, \mu_{i12h}^{n+1} = \mu_{i22h}^{n+1}$. Thus we only need to solve any one of these two systems. Meanwhile, by performing a derivation process similar to the proof of the second step of Theorem 3.1, the following conditions hold:

$$\begin{cases} \phi_{311h}^{n+1} = 1 - \phi_{111h}^{n+1} - \phi_{211h}^{n+1}, & \phi_{312h}^{n+1} = -\phi_{112h}^{n+1} - \phi_{212h}^{n+1}, \\ \phi_{321h}^{n+1} = -\phi_{121h}^{n+1} - \phi_{221h}^{n+1}, & \phi_{322h}^{n+1} = -\phi_{122h}^{n+1} - \phi_{222h}^{n+1}. \end{cases} \tag{3.68}$$

We set $w_h = 1$ in the four sub-systems (3.64)–(3.67) to obtain

$$\begin{aligned} &\int_\Omega \phi_{i11h}^{n+1} d\boldsymbol{x} = \int_\Omega \phi_{ih}^{n} d\boldsymbol{x} = \cdots = \int_\Omega \phi_{ih}^{0} d\boldsymbol{x} = \int_\Omega \phi_{i}^{*} d\boldsymbol{x}, \\ &\int_\Omega \phi_{i12h}^{n+1} d\boldsymbol{x} = \int_\Omega \phi_{i21h}^{n+1} d\boldsymbol{x} = \int_\Omega \phi_{i22h}^{n+1} d\boldsymbol{x} = 0, i = 1, 2, 3. \end{aligned} \tag{3.69}$$

Moreover, the practical implementation of the four linear systems (3.64)–(3.67) can be further simplified. By setting $w_h = \Theta_h$ and combine the two sub-equations in each subsystem together, (3.64)–(3.67) become

$$\begin{cases} \frac{a}{2M\delta t}(\phi_{i11h}^{n+1}, \Theta_h) + \frac{3}{4}\epsilon(\nabla\phi_{i11h}^{n+1}, \nabla\Theta_h) + \frac{S}{\epsilon}(\phi_{i11h}^{n+1}, \Theta_h) = G_{i1}, \\ \frac{a}{2M\delta t}(\phi_{i12h}^{n+1}, \Theta_h) + \frac{3}{4}\epsilon(\nabla\phi_{i12h}^{n+1}, \nabla\Theta_h) + \frac{S}{\epsilon}(\phi_{i12h}^{n+1}, \Theta_h) = G_{i2}, \\ \frac{a}{2M\delta t}(\phi_{i21h}^{n+1}, \Theta_h) + \frac{3}{4}\epsilon(\nabla\phi_{i21h}^{n+1}, \nabla\Theta_h) + \frac{S}{\epsilon}(\phi_{i21h}^{n+1}, \Theta_h) = G_{i3}, \\ \frac{a}{2M\delta t}(\phi_{i22h}^{n+1}, \Theta_h) - \frac{3}{4}\epsilon(\nabla\phi_{i22h}^{n+1}, \nabla\Theta_h) + \frac{S}{\epsilon}(\phi_{i22h}^{n+1}, \Theta_h) = G_{i4}, \end{cases} \tag{3.70}$$

where

$$\begin{cases} G_{i1} = (\frac{b\phi_i^n - c\phi_i^{n-1}}{2M\delta t} + \frac{S}{\epsilon}\phi_i^*, \Theta_h), \\ G_{i2} = -\frac{12}{\epsilon\Sigma_i}\left(H_i^* - \frac{1}{|\Omega|}\int_\Omega H_i^* d\boldsymbol{x} + \beta^* - \frac{1}{|\Omega|}\int_\Omega \beta^* d\boldsymbol{x}, \Theta_h\right), \\ G_{i3} = (\mathbf{u}^*(\phi_i^* - \hat{\phi}_i^0), \nabla\Theta_h), \ G_{i4} = G_{i2}. \end{cases} \tag{3.71}$$

We can directly solve the four independent elliptic equations in the system (3.70) to obtain ϕ_{i11h}^{n+1}, ϕ_{i12h}^{n+1}, ϕ_{i21h}^{n+1}, ϕ_{i22h}^{n+1}, $i = 1, 2, 3$ since all terms at the right-hand side of (3.70) are given explicitly. Note that all coefficients are constants, so solving them directly will be very efficient. Or one can solve ϕ_{i11h}^{n+1}, ϕ_{i12h}^{n+1}, ϕ_{i21h}^{n+1}, ϕ_{i22h}^{n+1} for $i = 1, 2$ from (3.70), and update ϕ_{311h}^{n+1}, ϕ_{312h}^{n+1}, ϕ_{321h}^{n+1}, ϕ_{322h}^{n+1} from (3.68). Once ϕ_{i11h}^{n+1}, ϕ_{i12h}^{n+1}, ϕ_{i21h}^{n+1}, ϕ_{i22h}^{n+1} with $i = 1, 2, 3$ are obtained, the variables μ_{i11h}^{n+1}, μ_{i12h}^{n+1}, μ_{i21h}^{n+1}, μ_{i22h}^{n+1} for $i = 1, 2, 3$ can be easily updated by using the second equation in the four sub-systems (3.64)–(3.67).

Step 2. Second, we rewrite (3.37) as the following form

$$U^{n+1} = \frac{1}{2}\sum_{i=1}^{3}(H_i^*, \phi_{ih}^{n+1}) + g^n, \tag{3.72}$$

where g^n is an explicit form that reads as

$$g^n = \frac{1}{a}(bU^n - cU^{n-1}) - \frac{1}{2a}\sum_{i=1}^{3}(H_i^*, b\phi_{ih}^n - c\phi_{ih}^{n-1}). \tag{3.73}$$

By substituting the linear form of U^{n+1}, ϕ_{ih}^{n+1} given in (3.57) into (3.72), we obtain

$$U_1^{n+1} + Q^{n+1}U_2^{n+1} = \frac{1}{2}\sum_{i=1}^{3}(H_i^*, \phi_{i1h}^{n+1} + Q^{n+1}\phi_{i2h}^{n+1}) + g^n. \tag{3.74}$$

Then, according to Q^{n+1}, we decompose (3.74) into the following two equalities:

$$\begin{cases} U_1^{n+1} = \frac{1}{2}\sum_{i=1}^{3}(H_i^*, \phi_{i1h}^{n+1}) + g^n, \\ U_2^{n+1} = \frac{1}{2}\sum_{i=1}^{3}(H_i^*, \phi_{i2h}^{n+1}). \end{cases} \tag{3.75}$$

Substituting the linear form of $(\phi_{i1h}, \phi_{i2h})^{n+1}$ given in (3.63) into (3.75), we get

$$\begin{cases} U_1^{n+1} = \frac{1}{2}\sum_{i=1}^{3}(H_i^*, \phi_{i11h}^{n+1} + U_1^{n+1}\phi_{i12h}^{n+1}) + g^n, \\ U_2^{n+1} = \frac{1}{2}\sum_{i=1}^{3}(H_i^*, \phi_{i21h}^{n+1} + U_2^{n+1}\phi_{i22h}^{n+1})d\boldsymbol{x}. \end{cases} \tag{3.76}$$

After applying a simple factorization to the two equations in (3.76), we derive

$$\begin{cases} U_1^{n+1} = \dfrac{\frac{1}{2}\sum_{i=1}^{3}(H_i^*, \phi_{i11h}^{n+1}) + g^n}{1 - \frac{1}{2}\sum_{i=1}^{3}(H_i^*, \phi_{i12h}^{n+1})}, \\ U_2^{n+1} = \dfrac{\frac{1}{2}\sum_{i=1}^{3}(H_i^*, \phi_{i21h}^{n+1})}{1 - \frac{1}{2}\sum_{i=1}^{3}(H_i^*, \phi_{i22h}^{n+1})}. \end{cases} \tag{3.77}$$

The solvability of U_1^{n+1} and U_2^{n+1}, i.e., the two denominators in (3.77) are not zero, are important, that can be proven rigorously by applying a simple energy estimation to the subsystem (3.65) or (3.67), as follows.

By setting $w_h = -\frac{2\delta t}{a}\mu_{i12h}^{n+1}$ and $\Theta_h = \phi_{i12h}^{n+1}$ in (3.65), combining the obtained equations, and taking the summation for $i = 1, 2, 3$, we derive

$$\begin{aligned} \frac{2M\delta t}{a}\sum_{i=1}^{3}\Sigma_i\left\|\frac{\bar{\mu}_{i12h}^{n+1}}{\Sigma_i}\right\|^2 + \frac{3}{4}\epsilon\sum_{i=1}^{3}\Sigma_i\|\nabla\phi_{i12h}^{n+1}\|^2 + \frac{S}{\epsilon}\sum_{i=1}^{3}\Sigma_i\|\phi_{i12h}^{n+1}\|^2 \\ = -\frac{12}{\epsilon}\left(\sum_{i=1}^{3}(H_i^*, \phi_{i12h}^{n+1}) + \sum_{i=1}^{3}(\beta^*, \phi_{i12h}^{n+1})\right). \end{aligned} \tag{3.78}$$

From $\phi_{112h}^{n+1} + \phi_{212h}^{n+1} + \phi_{312h}^{n+1} = 0$ that is given in (3.68), it is easy to derive $\frac{\mu_{112h}^{n+1}}{\Sigma_1} + \frac{\mu_{212h}^{n+1}}{\Sigma_2} + \frac{\mu_{312h}^{n+1}}{\Sigma_3} = 0$ by using (3.51). This implies $\frac{\bar{\mu}_{112h}^{n+1}}{\Sigma_1} + \frac{\bar{\mu}_{212h}^{n+1}}{\Sigma_2} + \frac{\bar{\mu}_{312h}^{n+1}}{\Sigma_3} = 0$. Hence, by using (2.19), we derive

$$\begin{cases} \displaystyle\sum_{i=1}^{3}\Sigma_i\left\|\frac{\bar{\mu}_{i12h}^{n+1}}{\Sigma_i}\right\|^2 \geq \underline{\Sigma}\sum_{i=1}^{3}\left\|\frac{\bar{\mu}_{i12h}^{n+1}}{\Sigma_i}\right\|^2 \geq 0, \\ \displaystyle\sum_{i=1}^{3}(\beta^*, \phi_{i12h}^{n+1}) = (\beta^*, \sum_{i=1}^{3}\phi_{i12h}^{n+1}) = 0, \\ \displaystyle\sum_{i=1}^{3}\Sigma_i\|\phi_{i12h}^{n+1}\|^2 \geq \underline{\Sigma}(\|\phi_{112h}^{n+1}\|^2 + \|\phi_{212h}^{n+1}\|^2 + \|\phi_{312h}^{n+1}\|^2) \geq 0, \\ \displaystyle\sum_{i=1}^{3}\Sigma_i\|\nabla\phi_{i12h}^{n+1}\|^2 \geq \underline{\Sigma}(\|\nabla\phi_{112h}^{n+1}\|^2 + \|\nabla\phi_{212h}^{n+1}\|^2 + \|\nabla\phi_{312h}^{n+1}\|^2) \geq 0. \end{cases} \tag{3.79}$$

Thus we obtain $-\sum_{i=1}^{3}(H_i^*, \phi_{i12h}^{n+1}) \geq 0$. This also means $-\sum_{i=1}^{3}(H_i^*, \phi_{i22h}^{n+1}) \geq 0$ since $\phi_{i12h}^{n+1} = \phi_{i22h}^{n+1}$. Hence, U_1^{n+1}, U_2^{n+1} given in (3.77) are uniquely solvable.

Step 3. Third, we use the nonlocal variable Q^{n+1} to split the velocity field $\tilde{\mathbf{u}}_h^{n+1}$ as the following form:

$$\tilde{\mathbf{u}}_h^{n+1} = \tilde{\mathbf{u}}_{1h}^{n+1} + Q^{n+1}\tilde{\mathbf{u}}_{2h}^{n+1}. \tag{3.80}$$

By replacing the variables $\tilde{\mathbf{u}}_h^{n+1}$ in (3.34), and then splitting the obtained equation according to Q^{n+1}, we arrive at a system that includes two linear elliptic sub-equations with constant coefficients as follows:

$$\begin{cases} \dfrac{a}{2\delta t}(\tilde{\mathbf{u}}_{1h}^{n+1}, \mathbf{v}_h) + \nu(\nabla\tilde{\mathbf{u}}_{1h}^{n+1}, \nabla\mathbf{v}_h) = (-\nabla p_h^n + \dfrac{b\mathbf{u}_h^n - c\mathbf{u}_h^{n-1}}{2\delta t}, \mathbf{v}_h), \\ \dfrac{a}{2\delta t}(\tilde{\mathbf{u}}_{2h}^{n+1}, \mathbf{v}_h) + \nu(\nabla\tilde{\mathbf{u}}_{2h}^{n+1}, \nabla\mathbf{v}_h) = (-(\mathbf{u}^*\cdot\nabla)\mathbf{u}^* - \lambda\displaystyle\sum_{i=1}^{3}(\phi_i^* - \hat{\phi}_i^0)\nabla\mu_i^*, \mathbf{v}_h). \end{cases} \tag{3.81}$$

Step 4. Fourth, we solve the auxiliary variable Q^{n+1}. Using the split form for the variables $\tilde{\mathbf{u}}_h^{n+1}$ in (3.80) and μ_{ih}^{n+1} in (3.57), one can rewrite the scheme (3.38) as the following form:

$$(\frac{a}{2\delta t} - \vartheta_2)Q^{n+1} = \frac{1}{2\delta t}(bQ^n - cQ^{n-1}) + \vartheta_1, \tag{3.82}$$

where

$$\begin{cases} \vartheta_1 = -\lambda\sum_{i=1}^{3}(\mathbf{u}^*(\phi_i^* - \hat{\phi}_i^0), \nabla\mu_{i1h}^{n+1}) + \lambda\sum_{i=1}^{3}((\phi_i^* - \hat{\phi}_i^0)\nabla\mu_i^*, \tilde{\mathbf{u}}_{1h}^{n+1}) + ((\mathbf{u}^*\cdot\nabla)\mathbf{u}^*, \tilde{\mathbf{u}}_{1h}^{n+1}), \\ \vartheta_2 = -\lambda\sum_{i=1}^{3}(\mathbf{u}^*(\phi_i^* - \hat{\phi}_i^0), \nabla\mu_{i2h}^{n+1}) + \lambda\sum_{i=1}^{3}((\phi_i^* - \hat{\phi}_i^0)\nabla\mu_i^*, \tilde{\mathbf{u}}_{2h}^{n+1}) + ((\mathbf{u}^*\cdot\nabla)\mathbf{u}^*, \tilde{\mathbf{u}}_{2h}^{n+1}). \end{cases} \tag{3.83}$$

The solvability of (3.82) is also important and it can be proven by showing $\frac{a}{2\delta t} - \vartheta_2 \neq 0$ as follows. By setting $\mathbf{v}_h = \tilde{\mathbf{u}}_{2h}^{n+1}$ in the second equation of (3.81), we get

$$-((\mathbf{u}^*\cdot\nabla)\mathbf{u}^*, \tilde{\mathbf{u}}_{2h}^{n+1}) - \lambda(\sum_{i=1}^{3}(\phi_i^* - \hat{\phi}_i^0)\nabla\mu_i^*, \tilde{\mathbf{u}}_{2h}^{n+1}) = \frac{a}{2\delta t}\|\tilde{\mathbf{u}}_{2h}^{n+1}\|^2 + \nu\|\nabla\tilde{\mathbf{u}}_{2h}^{n+1}\|^2 \geq 0. \tag{3.84}$$

By setting $w_h = -\mu_{i2h}^{n+1}$ and $\Theta_h = \frac{a}{2\delta t}\phi_{i2h}^{n+1}$ in (3.60), and combining the two obtained equations and taking the summation for $i = 1, 2, 3$, we derive

$$\begin{aligned} \sum_{i=1}^{3}(\mathbf{u}^*(\phi_i^* - \hat{\phi}_i^0), \nabla\mu_{i2h}^{n+1}) =& M\sum_{i=1}^{3}\Sigma_i\left\|\frac{\bar{\mu}_{i2h}^{n+1}}{\Sigma_i}\right\|^2 + \frac{3a\epsilon}{8\delta t}\sum_{i=1}^{3}\Sigma_i\|\nabla\phi_{i2h}^{n+1}\|^2 \\ &+ \frac{aS}{2\epsilon\delta t}\sum_{i=1}^{3}\Sigma_i\|\phi_{i2h}^{n+1}\|^2 + \frac{12a}{2\epsilon\delta t}U_2^{n+1}\sum_{i=1}^{3}(H_i^*, \phi_{i2h}^{n+1}) \\ &+ \frac{12a}{2\epsilon\delta t}U_2^{n+1}(\beta^*, \sum_{i=1}^{3}\phi_{i2h}^{n+1}). \end{aligned} \tag{3.85}$$

From the second equation of (3.75), we get

$$U_2^{n+1}\sum_{i=1}^{3}(H_i^*, \phi_{i2h}^{n+1}) = \frac{1}{2}\Big(\sum_{i=1}^{3}(H_i^*, \phi_{i2}^{n+1})\Big)^2 \geq 0. \tag{3.86}$$

By using (3.61) and (2.19), we derive

$$\begin{aligned} &\sum_{i=1}^{3}\Sigma_i\left\|\frac{\bar{\mu}_{i2h}^{n+1}}{\Sigma_i}\right\|^2 \geq \underline{\Sigma}\sum_{i=1}^{3}\left\|\frac{\bar{\mu}_{i2h}^{n+1}}{\Sigma_i}\right\|^2 \geq 0, \qquad \sum_{i=1}^{3}\Sigma_i\|\nabla\phi_{i2h}^{n+1}\|^2 \geq \underline{\Sigma}\sum_{i=1}^{3}\|\nabla\phi_{i2h}^{n+1}\|^2 \geq 0, \\ &\sum_{i=1}^{3}\Sigma_i\|\phi_{i2h}^{n+1}\|^2 \geq \underline{\Sigma}\sum_{i=1}^{3}\|\phi_{i2h}^{n+1}\|^2 \geq 0, \qquad (\beta^*, \sum_{i=1}^{3}\phi_{i2h}^{n+1}) = 0. \end{aligned} \tag{3.87}$$

Hence, we derive

$$\sum_{i=1}^{3}(\mathbf{u}^*(\phi_i^* - \hat{\phi}_i^0), \nabla\mu_{i2h}^{n+1}) \geq 0. \tag{3.88}$$

Therefore, (3.84) and (3.88) imply that $-\vartheta_2 \geq 0$, thereby ensuring the solvability of (3.82).

Step 4. Finally, we update ϕ_{ih}^{n+1}, μ_{ih}^{n+1} for $i = 1, 2, 3$ and U^{n+1} from (3.57), $\tilde{\mathbf{u}}_h^{n+1}$ from (3.80), and $\mathbf{u}_h^{n+1}$, p_h^{n+1} from (3.39)–(3.40).

Therefore, to summarize, by using the nonlocal variables Q^{n+1} and U^{n+1}, and the splitting technique, we arrive at the full decoupling implementation method of the proposed scheme (3.34)–(3.40). At each step, we only need to solve a series of independent elliptic equations. Moreover, all these equations are linear, fully-decoupled, and only have constant coefficients, which means very efficient calculations in practice.

Remark 3.7. For the sake of completeness, here we present the stabilized-explicit method (cf. [24–27]) that is another widely used fully-decoupled type scheme for Navier–Stokes coupled phase-field model. For simplicity, we only consider the two-phasic case (i.e., let $\phi = \phi_1 = 1 - \phi_2$, $\phi_3 = 0$), and only discretize the related terms in time,

while other terms remain continuously so that the readers can see more clearly. The scheme reads as

$$\begin{cases} \dfrac{\phi^{n+1}-\phi^n}{\delta t} + ((\mathbf{u}^n \underbrace{-\delta t \phi^n \nabla \mu^{n+1}}_{\text{stabilization term}}) \cdot \nabla)\phi^n + \bar{\mu}^{n+1} = 0, \\ \dfrac{\mathbf{u}^{n+1}-\mathbf{u}^n}{\delta t} + (\mathbf{u}\cdot\nabla)\mathbf{u} - \nu\Delta\mathbf{u} + \nabla p + \underbrace{\lambda\phi^n\nabla\mu^{n+1}}_{\text{explicit since } \mu^{n+1} \text{ is obtained above}} = 0, \end{cases} \tag{3.89}$$

We can see that the scheme (3.89) is a fully-decoupled and linear scheme, but the added stabilization term in the advection contains the implicit processed potential μ^{n+1}, so it is necessary to solve the phase-field equation with variable coefficients at each time step. In addition, this scheme only has a first-order version. Compared with it, the scheme (3.35)–(3.40) developed in this paper is fully-decoupled, second-order in time, and only needs to solve equations with constant coefficients, which illustrates very high efficiency in practice.

Except for the above-listed scheme, we also recall some positivity preserved schemes developed in [38,39] for the flow-coupled conserved Allen–Cahn type two-phasic model. Those schemes are fully-coupled type, however, they are only energy stable when the fluid velocity vanishes.

3.4. Unconditional energy stability

In this subsection, we show the fully discrete scheme follows unconditional energy stability. We will use the following two identities repeatedly:

$$2(3a-4b+c)a = |a|^2 - |b|^2 + |2a-b|^2 - |2b-c|^2 + |a-2b+c|^2, \tag{3.90}$$

$$(3a-4b+c)(a-2b+c) = |a-b|^2 - |b-c|^2 + 2|a-2b+c|^2. \tag{3.91}$$

Theorem 3.2. *If (2.20) holds, then the scheme (3.34)–(3.40) satisfies the following discrete energy dissipation law:*

$$\frac{1}{\delta t}(E_h^{n+1} - E_h^n) \le -\nu\|\nabla\tilde{\mathbf{u}}_h^{n+1}\|^2 - \lambda M \underline{\Sigma} \sum_{i=1}^{3} \left\| \frac{\bar{\mu}_{ih}^{n+1}}{\Sigma_i} \right\|^2 \le 0, \tag{3.92}$$

where

$$\begin{aligned} E_h^{n+1} =& \frac{1}{2}\Big(\frac{1}{2}\|\mathbf{u}_h^{n+1}\|^2 + \frac{1}{2}\|2\mathbf{u}_h^{n+1} - \mathbf{u}_h^n\|^2\Big) + \frac{\delta t^2}{3}\|\nabla p_h^{n+1}\|^2 \\ &+ \lambda\frac{3\epsilon}{8}\sum_{i=1}^{3}\left(\Sigma_i\Big(\frac{1}{2}\|\nabla\phi_{ih}^{n+1}\|^2 + \frac{1}{2}\|2\nabla\phi_{ih}^{n+1} - \nabla\phi_{ih}^n\|^2\Big)\right) \\ &+ \lambda\frac{12}{\epsilon}\Big(\frac{1}{2}|U^{n+1}|^2 + \frac{1}{2}|2U^{n+1} - U^n|^2\Big) + \frac{1}{2}\Big(\frac{1}{2}|Q^{n+1}|^2 + \frac{1}{2}|2Q^{n+1} - Q^n|^2\Big) \\ &+ \lambda\frac{S}{2\epsilon}\sum_{i=1}^{3}(\Sigma_i\|\phi_{ih}^{n+1} - \phi_{ih}^n\|^2) \ge 0. \end{aligned} \tag{3.93}$$

Proof. We first show $E_h^{n+1} \ge 0$. Since (2.20) holds, from (2.19) and (3.47), we derive

$$\begin{cases} \displaystyle\sum_{i=1}^{3}\Sigma_i\|\nabla\phi_{ih}^{n+1}\|^2 \ge \underline{\Sigma}\sum_{i=1}^{3}\|\nabla\phi_{ih}^{n+1}\|^2 \ge 0, \\ \displaystyle\sum_{i=1}^{3}\Sigma_i\|2\nabla\phi_{ih}^{n+1} - \nabla\phi_{ih}^n\|^2 \ge \underline{\Sigma}\sum_{i=1}^{3}\|2\nabla\phi_{ih}^{n+1} - \nabla\phi_{ih}^n\|^2 \ge 0, \\ \displaystyle\sum_{i=1}^{3}\Sigma_i\|\phi_{ih}^{n+1} - \phi_{ih}^n\|^2 \ge \underline{\Sigma}\sum_{i=1}^{3}\|\phi_{ih}^{n+1} - \phi_{ih}^n\|^2 \ge 0, \end{cases} \tag{3.94}$$

which implies $E_h^{n+1} \ge 0$.

We continue to show the energy law (3.92) holds.

By taking $\mathbf{v}_h = 2\delta t\tilde{\mathbf{u}}_h^{n+1}$ in (3.34), we obtain

$$\begin{aligned}&(3\tilde{\mathbf{u}}_h^{n+1} - 4\mathbf{u}_h^n + \mathbf{u}_h^{n-1}, \tilde{\mathbf{u}}_h^{n+1}) + 2\nu\delta t\|\nabla\tilde{\mathbf{u}}_h^{n+1}\|^2 + 2\delta t(\nabla p_h^n, \tilde{\mathbf{u}}_h^{n+1})\\ &\quad = -2\delta t\, Q^{n+1}((\mathbf{u}^*\cdot\nabla)\mathbf{u}^*, \tilde{\mathbf{u}}_h^{n+1}) - 2\delta t\lambda Q^{n+1}\sum_{i=1}^{3}(\phi_i^*\nabla\mu_i^*, \tilde{\mathbf{u}}_h^{n+1}).\end{aligned} \tag{3.95}$$

We rewrite (3.40) as

$$\tilde{\mathbf{u}}_h^{n+1} - \mathbf{u}_h^{n+1} = \frac{2\delta t}{3}\nabla(p_h^{n+1} - p_h^n). \tag{3.96}$$

Taking the L^2 inner product of the above equality with $\mathbf{u}_h^{n+1}$, we derive

$$(\tilde{\mathbf{u}}_h^{n+1} - \mathbf{u}_h^{n+1}, \mathbf{u}_h^{n+1}) = \frac{2\delta t}{3}(\nabla(p_h^{n+1} - p_h^n), \mathbf{u}_h^{n+1}) = 0, \tag{3.97}$$

and

$$\begin{aligned}&(3\mathbf{u}_h^{n+1} - 4\mathbf{u}_h^n + \mathbf{u}_h^{n-1}, \tilde{\mathbf{u}}_h^{n+1} - \mathbf{u}_h^{n+1})\\ &\quad = (3\mathbf{u}_h^{n+1} - 4\mathbf{u}_h^n + \mathbf{u}_h^{n-1}, \frac{2\delta t}{3}\nabla(p_h^{n+1} - p_h^n)) = 0,\end{aligned} \tag{3.98}$$

where (3.43) is used. By using (3.97) and (3.98), we deduce

$$\begin{aligned}&(3\tilde{\mathbf{u}}_h^{n+1} - 4\mathbf{u}_h^n + \mathbf{u}_h^{n-1}, \tilde{\mathbf{u}}_h^{n+1})\\ &\quad = \big(3\tilde{\mathbf{u}}_h^{n+1} - 3\mathbf{u}_h^{n+1}, \tilde{\mathbf{u}}_h^{n+1}\big) + \big(3\mathbf{u}_h^{n+1} - 4\mathbf{u}_h^n + \mathbf{u}_h^{n-1}, \tilde{\mathbf{u}}_h^{n+1}\big)\\ &\quad = \big(3\tilde{\mathbf{u}}_h^{n+1} - 3\mathbf{u}_h^{n+1}, \tilde{\mathbf{u}}_h^{n+1} + \mathbf{u}_h^{n+1}\big) + \big(3\mathbf{u}_h^{n+1} - 4\mathbf{u}_h^n + \mathbf{u}_h^{n-1}, \mathbf{u}_h^{n+1}\big)\\ &\quad = \frac{1}{2}(\|\mathbf{u}_h^{n+1}\|^2 - \|\mathbf{u}_h^n\|^2 + \|2\mathbf{u}_h^{n+1} - \mathbf{u}_h^n\|^2 - \|2\mathbf{u}_h^n - \mathbf{u}_h^{n-1}\|^2 + \|\mathbf{u}_h^{n+1} - 2\mathbf{u}_h^n + \mathbf{u}_h^{n-1}\|^2)\\ &\qquad + 3\|\tilde{\mathbf{u}}_h^{n+1}\|^2 - 3\|\mathbf{u}_h^{n+1}\|^2.\end{aligned} \tag{3.99}$$

We rewrite (3.40) as

$$\mathbf{u}_h^{n+1} + \frac{2}{3}\delta t\nabla p_h^{n+1} = \tilde{\mathbf{u}}_h^{n+1} + \frac{2}{3}\delta t\nabla p_h^n.$$

Taking the L^2 inner product of the above equation with itself and multiply the result with $\frac{3}{2}$, we derive

$$2\delta t(\tilde{\mathbf{u}}_h^{n+1}, \nabla p_h^n) = \frac{3}{2}\|\mathbf{u}_h^{n+1}\|^2 - \frac{3}{2}\|\tilde{\mathbf{u}}_h^{n+1}\|^2 + \frac{2\delta t^2}{3}\|\nabla p_h^{n+1}\|^2 - \frac{2\delta t^2}{3}\|\nabla p_h^n\|^2. \tag{3.100}$$

We rewrite (3.40) as

$$\mathbf{u}_h^{n+1} - \tilde{\mathbf{u}}_h^{n+1} = -\frac{2}{3}\delta t\nabla p_h^{n+1} + \frac{2}{3}\delta t\nabla p_h^n. \tag{3.101}$$

By taking the L^2 inner product of the above equation with $\frac{3}{2}\mathbf{u}_h^{n+1}$ and using (3.43), we obtain

$$\frac{3}{2}\|\mathbf{u}_h^{n+1} - \tilde{\mathbf{u}}_h^{n+1}\|^2 + \frac{3}{2}\|\mathbf{u}_h^{n+1}\|^2 = \frac{3}{2}\|\tilde{\mathbf{u}}_h^{n+1}\|^2. \tag{3.102}$$

We combine (3.95), (3.99), (3.100), and (3.102) to obtain

$$\begin{aligned}&\frac{1}{2}(\|\mathbf{u}_h^{n+1}\|^2 - \|\mathbf{u}_h^n\|^2 + \|2\mathbf{u}_h^{n+1} - \mathbf{u}_h^n\|^2 - \|2\mathbf{u}_h^n - \mathbf{u}_h^{n-1}\|^2 + \|\mathbf{u}_h^{n+1} - 2\mathbf{u}_h^n + \mathbf{u}_h^{n-1}\|^2)\\ &\qquad + \frac{3}{2}\|\mathbf{u}_h^{n+1} - \tilde{\mathbf{u}}_h^{n+1}\|^2 + \frac{2\delta t^2}{3}(\|\nabla p_h^{n+1}\|^2 - \|\nabla p_h^n\|^2) + 2\nu\delta t\|\nabla\tilde{\mathbf{u}}_h^{n+1}\|^2\\ &\quad = -2\delta t\, Q^{n+1}((\mathbf{u}^*\cdot\nabla)\mathbf{u}^*, \tilde{\mathbf{u}}_h^{n+1}) - 2\delta t\lambda Q^{n+1}\sum_{i=1}^{3}((\phi_i^* - \hat{\phi}_i^0)\nabla\mu_i^*, \tilde{\mathbf{u}}_h^{n+1}).\end{aligned} \tag{3.103}$$

By setting $w_h = 2\delta t\lambda\mu_{ih}^{n+1}$ in (3.35) and taking the summation for the obtained equations for $i = 1, 2, 3$, we derive

$$\begin{aligned}\lambda\sum_{i=1}^{3}(3\phi_{ih}^{n+1}-4\phi_{ih}^{n}+\phi_{ih}^{n-1},\mu_{ih}^{n+1})+2\delta t\lambda M\sum_{i=1}^{3}\Sigma_i\left\|\frac{\bar{\mu}_{ih}^{n+1}}{\Sigma_i}\right\|^2\\ =2\delta t\lambda Q^{n+1}\sum_{i=1}^{3}(\mathbf{u}^*(\phi_i^*-\hat{\phi}_i^0),\nabla\mu_{ih}^{n+1}).\end{aligned}\tag{3.104}$$

By setting $\Theta_h = -\lambda(3\phi_{ih}^{n+1}-4\phi_{ih}^{n}+\phi_{ih}^{n-1})$ in (3.36) and taking the summation for the obtained equations for $i = 1, 2, 3$, we get

$$\begin{aligned}-\lambda\sum_{i=1}^{3}(\mu_{ih}^{n+1},3\phi_{ih}^{n+1}-4\phi_{ih}^{n}+\phi_{ih}^{n-1})+\frac{3}{4}\epsilon\lambda\sum_{i=1}^{3}\Sigma_i(\nabla\phi_{ih}^{n+1},\nabla(3\phi_{ih}^{n+1}-4\phi_{ih}^{n}+\phi_{ih}^{n-1}))\\ =-\lambda\frac{12}{\epsilon}U^{n+1}\sum_{i=1}^{3}(H_i^*,3\phi_{ih}^{n+1}-4\phi_{ih}^{n}+\phi_{ih}^{n-1})\\ -\lambda\frac{S}{\epsilon}\sum_{i=1}^{3}\Sigma_i\big(\phi_{ih}^{n+1}-\phi_i^*,3\phi_{ih}^{n+1}-4\phi_{ih}^{n}+\phi_{ih}^{n-1}\big),\end{aligned}\tag{3.105}$$

where the term $\lambda\frac{12}{\epsilon}U^{n+1}\sum_{i=1}^{3}(\beta^*,3\phi_{ih}^{n+1}-4\phi_{ih}^{n}+\phi_{ih}^{n-1})$ vanishes by using $\sum_{i=1}^{3}(3\phi_{ih}^{n+1}-4\phi_{ih}^{n}+\phi_{ih}^{n-1})=3-4+1=0$ that is due to (3.47).

Multiplying (3.37) with $\lambda\frac{24}{\epsilon}U^{n+1}$ and using (3.90), we obtain

$$\begin{aligned}\lambda\frac{12}{\epsilon}\Big(|U^{n+1}|^2-|U^n|^2+|2U^{n+1}-U^n|^2-|2U^n-U^{n-1}|^2+|U^{n+1}-2U^n+U^{n-1}|^2\Big)\\ =\lambda\frac{12}{\epsilon}U^{n+1}\sum_{i=1}^{3}(H_i^*,3\phi_{ih}^{n+1}-4\phi_{ih}^{n}+\phi_{ih}^{n-1}).\end{aligned}\tag{3.106}$$

Multiplying (3.38) with $2\delta t\,Q^{n+1}$ and using (3.90), we obtain

$$\begin{aligned}\frac{1}{2}\Big(|Q^{n+1}|^2-|Q^n|^2+|2Q^{n+1}-Q^n|^2-|2Q^n-Q^{n-1}|^2+|Q^{n+1}-2Q^n+Q^{n-1}|^2\Big)\\ =-2\lambda\delta t\,Q^{n+1}\sum_{i=1}^{3}(\mathbf{u}^*(\phi_i^*-\hat{\phi}_i^0),\nabla\mu_{ih}^{n+1})+2\lambda\delta t\,Q^{n+1}\sum_{i=1}^{3}((\phi_i^*-\hat{\phi}_i^0)\nabla\mu_i^*,\tilde{\mathbf{u}}_h^{n+1})\\ +2\delta t\,Q^{n+1}((\mathbf{u}^*\cdot\nabla)\mathbf{u}^*,\tilde{\mathbf{u}}_h^{n+1}).\end{aligned}\tag{3.107}$$

Hence, by combining (3.103)–(3.107) and using (3.91), we get

$$\begin{aligned}&\frac{1}{2}(\|\mathbf{u}_h^{n+1}\|^2-\|\mathbf{u}_h^n\|^2+\|2\mathbf{u}_h^{n+1}-\mathbf{u}_h^n\|^2-\|2\mathbf{u}_h^n-\mathbf{u}_h^{n-1}\|^2)+\frac{2\delta t^2}{3}(\|\nabla p_h^{n+1}\|^2-\|\nabla p_h^n\|^2)\\ &+\lambda\frac{3\epsilon}{8}\sum_{i=1}^{3}\Big(\Sigma_i(\|\nabla\phi_{ih}^{n+1}\|^2-\|\nabla\phi_{ih}^n\|^2+\|\nabla(2\phi_{ih}^{n+1}-\phi_{ih}^n)\|^2-\|\nabla(2\phi_{ih}^n-\phi_{ih}^{n-1})\|^2)\Big)\\ &+\lambda\frac{12}{\epsilon}\Big(|U^{n+1}|^2-|U^n|^2+|2U^{n+1}-U^n|^2-|2U^n-U^{n-1}|^2\Big)\\ &+\frac{1}{2}\Big(|Q^{n+1}|^2-|Q^n|^2+|2Q^{n+1}-Q^n|^2-|2Q^n-Q^{n-1}|^2\Big)\\ &+\lambda\frac{S}{\epsilon}\sum_{i=1}^{3}\Big(\Sigma_i\left(\|\phi_{ih}^{n+1}-\phi_{ih}^n\|^2-\|\phi_{ih}^n-\phi_{ih}^{n-1}\|^2\right)\Big)+\chi_1=\chi_2,\end{aligned}\tag{3.108}$$

where

$$\begin{cases} \chi_1 = \dfrac{1}{2}\|\mathbf{u}_h^{n+1} - 2\mathbf{u}_h^n + \mathbf{u}_h^{n-1}\|^2 + \dfrac{3}{2}\|\mathbf{u}_h^{n+1} - \tilde{\mathbf{u}}_h^{n+1}\|^2 \\ \qquad + \lambda\dfrac{3\epsilon}{8}\displaystyle\sum_{i=1}^{3}\Sigma_i\|\nabla(\phi_{ih}^{n+1} - 2\phi_{ih}^n + \phi_{ih}^{n-1})\|^2 \\ \qquad + \lambda\dfrac{12}{\epsilon}|U^{n+1} - 2U^n + U^{n-1}|^2 + \dfrac{1}{2}|Q^{n+1} - 2Q^n + Q^{n-1}|^2 \\ \qquad + \lambda\dfrac{2S}{\epsilon}\displaystyle\sum_{i=1}^{3}\Sigma_i\|\phi_{ih}^{n+1} - 2\phi_{ih}^n + \phi_{ih}^{n-1}\|^2, \\ \chi_2 = -2\delta t\nu\|\nabla\tilde{\mathbf{u}}_h^{n+1}\|^2 - 2\lambda\delta t M\displaystyle\sum_{i=1}^{3}\Sigma_i\left\|\frac{\bar{\mu}_{ih}^{n+1}}{\Sigma_i}\right\|^2. \end{cases} \tag{3.109}$$

From (3.47) and (2.19), we derive

$$\begin{cases} \displaystyle\sum_{i=1}^{3}\Sigma_i\|\nabla(\phi_{ih}^{n+1} - 2\phi_{ih}^n + \phi_{ih}^{n-1})\|^2 \geq \underline{\Sigma}\sum_{i=1}^{3}\|\nabla(\phi_{ih}^{n+1} - 2\phi_{ih}^n + \phi_{ih}^{n-1})\|^2 \geq 0, \\ \displaystyle\sum_{i=1}^{3}\Sigma_i\|\phi_{ih}^{n+1} - 2\phi_{ih}^n + \phi_{ih}^{n-1}\|^2 \geq \underline{\Sigma}\sum_{i=1}^{3}\|\phi_{ih}^{n+1} - 2\phi_{ih}^n + \phi_{ih}^{n-1}\|^2 \geq 0, \end{cases} \tag{3.110}$$

which means

$$\chi_1 \geq 0. \tag{3.111}$$

From (3.49) and (2.19), we derive

$$\chi_2 \leq -2\delta t\nu\|\nabla\tilde{\mathbf{u}}_h^{n+1}\|^2 - 2\lambda\delta t M\underline{\Sigma}\sum_{i=1}^{3}\left\|\frac{\bar{\mu}_{ih}^{n+1}}{\Sigma_i}\right\|^2 \leq 0. \tag{3.112}$$

Finally, by dropping χ_1 in (3.108) and using (3.112), it is easy to see that (3.108) becomes

$$\begin{aligned} &\frac{1}{2}(\|\mathbf{u}_h^{n+1}\|^2 - \|\mathbf{u}_h^n\|^2 + \|2\mathbf{u}_h^{n+1} - \mathbf{u}_h^n\|^2 - \|2\mathbf{u}_h^n - \mathbf{u}_h^{n-1}\|^2) + \frac{2\delta t^2}{3}(\|\nabla p_h^{n+1}\|^2 - \|\nabla p_h^n\|^2) \\ &\quad + \lambda\frac{3\epsilon}{8}\sum_{i=1}^{3}\Big(\Sigma_i(\|\nabla\phi_{ih}^{n+1}\|^2 - \|\nabla\phi_{ih}^n\|^2 + \|\nabla(2\phi_{ih}^{n+1} - \phi_{ih}^n)\|^2 - \|\nabla(2\phi_{ih}^n - \phi_{ih}^{n-1})\|^2)\Big) \\ &\quad + \lambda\frac{12}{\epsilon}\Big(|U^{n+1}|^2 - |U^n|^2 + |2U^{n+1} - U^n|^2 - |2U^n - U^{n-1}|^2\Big) \\ &\quad + \frac{1}{2}\Big(|Q^{n+1}|^2 - |Q^n|^2 + |2Q^{n+1} - Q^n|^2 - |2Q^n - Q^{n-1}|^2\Big) \\ &\quad + \lambda\frac{S}{\epsilon}\sum_{i=1}^{3}\Big(\Sigma_i\left(\|\phi_{ih}^{n+1} - \phi_{ih}^n\|^2 - \|\phi_{ih}^n - \phi_{ih}^{n-1}\|^2\right)\Big) \\ &\quad \leq -2\delta t\nu\|\nabla\tilde{\mathbf{u}}_h^{n+1}\|^2 - 2\lambda\delta t M\underline{\Sigma}\sum_{i=1}^{3}\left\|\frac{\bar{\mu}_{ih}^{n+1}}{\Sigma_i}\right\|^2 \leq 0, \end{aligned} \tag{3.113}$$

which implies (3.92). □

Remark 3.8. Note that $\frac{1}{\delta t}(E_h^{n+1} - E_h^n)$ is the second-order approximation of the term $\frac{d}{dt}E(u,\phi)$ at $t = t^{n+1}$. Since for any smooth variable ψ with time, we always have the following heuristic approximations as

$$\begin{aligned} &\frac{\|\psi^{n+1}\|^2 + \|2\psi^{n+1} - \psi^n\|^2}{2\delta t} - \frac{\|\psi^n\|^2 + \|2\psi^n - \psi^{n-1}\|^2}{2\delta t} \\ &\qquad \cong \frac{\|\psi^{n+2}\|^2 - \|\psi^n\|^2}{2\delta t} + O(\delta t^2) \cong \frac{d}{dt}\|\psi(t^{n+1})\|^2 + O(\delta t^2). \end{aligned} \tag{3.114}$$

and

$$\frac{\|\psi^{n+1}-\psi^{n}\|^2-\|\psi^{n}-\psi^{n-1}\|^2}{2\delta t}\cong O(\delta t^2). \tag{3.115}$$

4. Numerical simulation

In this section, we perform various numerical simulations to testify the accuracy, stability, and effectiveness of the proposed algorithm (3.34)–(3.40) which is denoted as DSAV for convenience. We use Taylor–Hood element [78] for $\boldsymbol{V}_h$ and O_h that satisfies inf–sup condition and set the finite element spaces (3.26) with $l_1=1, l_2=2, l_3=1$. And the obtained linear systems are solved by using the conjugate gradient method. The low computational cost in these simulations also well demonstrates the efficiency of the proposed method. For example, the computation time cost of each time step of 2D example 4.2 is about 0.1 s, while the computation time of each time step of 3D example 4.3 is about 2.5 s.

4.1. Accuracy and stability tests

In this subsection, we test the convergence and stability of the developed scheme (3.34)–(3.40). We set the computed domain as $(x, y)\in\Omega=[0,1]\times[0,0.5]$. The initial conditions are set as follows

$$\begin{cases}\phi_i^0(x,y)=\tanh\left(\dfrac{r-\sqrt{(x-x_i)^2+(y-y_i)^2}}{\epsilon}\right), i=1,2, \phi_3^0=1-\phi_1^0-\phi_2^0,\\ \mathbf{u}^0=(u^0,v^0)=(0,0),\ p^0=0,\end{cases} \tag{4.1}$$

where $\epsilon=0.04$, $r=0.2$, $x_1=0.72$, $x_2=0.28$, and $y_1=y_2=0.25$. The model parameters are set as

$$M=1,\nu=1,\Lambda=1,B=10,S=4,\lambda=0.01,(\sigma_{12},\sigma_{13},\sigma_{23})=(1,1,1). \tag{4.2}$$

We first verify the spatial convergence order by plotting the error in various norms which are computed using various grid size h. We choose δt to be small enough ($\delta t=$ 1e−5) so that the errors are only dominated by the spatial discretization error. Since the exact solution is not known, we assume that the numerical solution calculated with a very tiny grid size $h=\frac{1}{512}$ is used as the approximate exact solution and refine the grid size h to test the spatial accuracy. The numerical errors between the numerical solution of the exact solution at $t=1$ are plotted in Fig. 4.1(a). We can see that the second-order convergence rate is followed by the H^1-error for the velocity, L^2-error of the pressure p, and L^2-error of the three phase-field variables. The third-order convergence rate is observed for L^2 error of the velocity. These results are in full agreement with the theoretical expectation of accuracy for $P2/P1$ element of $(\mathbf{u}, p)$ and $P1$ element of ϕ_i.

In Fig. 4.1(b), we continue to verify the temporal convergence order by fixing the grid size $h=\frac{1}{512}$. In this way, the spatial grid size is small enough and the spatial discretization errors are negligible compared to the time discretization error. The L^2-errors between the numerical solution of the exact solution (computed solution using a very tiny step size $\delta t=$ 1e−7) at $t=1$ are plotted, where various time step sizes are used. It can be observed that the scheme DSAV gives the second-order time accuracy of the velocity field and the average of ϕ_i, and the first-order time accuracy of p (note that the pressure is only first-order accurate for the particular projection type scheme used in this article due to the boundary layer phenomenon, see the theoretical/numerical evidence in [9,79,90,91]).

Using the same example, we further verify whether the DSAV scheme maintains energy stability. In Fig. 4.2, we plot the evolution curves of the total free energy (3.93) calculated by the scheme DSAV, where we use $h=\frac{1}{256}$, vary the time step size δt, and use two different sets of surface tension parameters $(\sigma_{12},\sigma_{13},\sigma_{23})=(1,1,1)$ and $(1,3,1)$. We find that all obtained energy curves show monotonic attenuation, which confirms the unconditional stability of DSAV. When the time step is relatively large, the energy curve with a large time step has an observable deviation from the energy curve with a small time step. This is because larger time steps lead to larger errors. When the time step is small, the obtained energy curves are very close, which indicates that these energy curves are getting closer to the exact solution.

To show the effectiveness of the extra stabilization term S, in Fig. 4.2(b), we append a small inset subfigure to plot the energy evolution curves calculated by the scheme DSAV but setting the stabilization parameter to be $S=0$. We find that the energy decays only for small time steps, i.e., $\delta t\le 0.01/2^4$. This phenomenon illustrates the

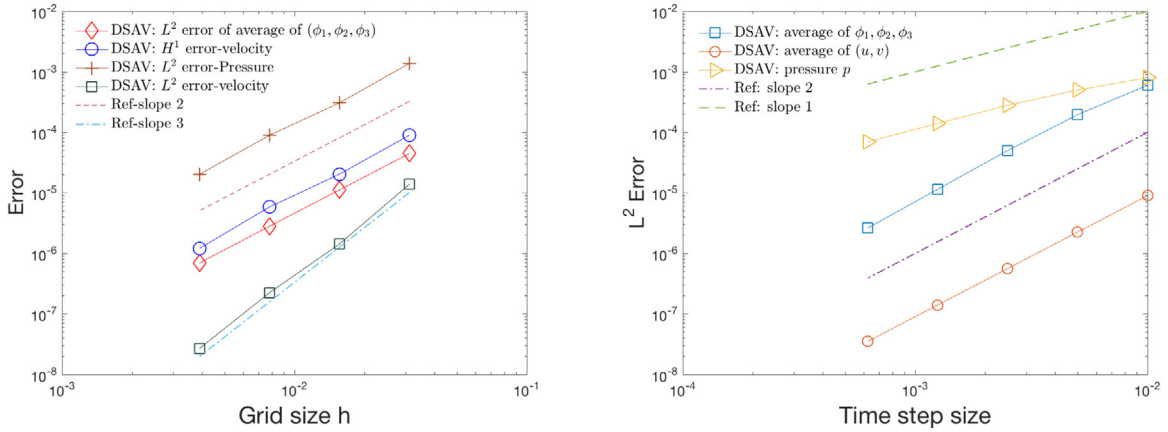

(a) Spatial error. (b) Temporal error.

Fig. 4.1. Convergence order of all unknown variables that are computed by using the various grid sizes and time steps.

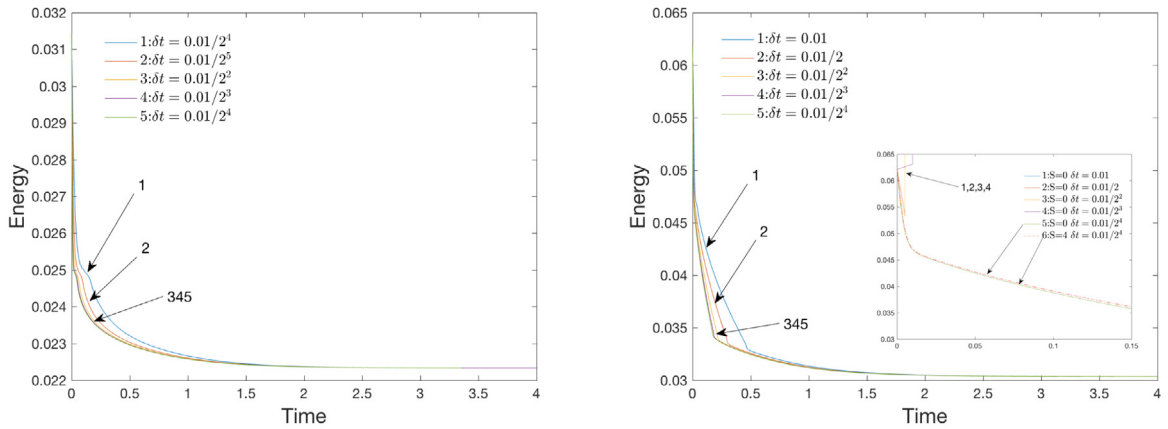

(a) $(\sigma_{12}, \sigma_{13}, \sigma_{23}) = (1, 1, 1)$. (b) $(\sigma_{12}, \sigma_{13}, \sigma_{23}) = (1, 3, 1)$.

Fig. 4.2. The time evolution of the total free energy (3.93) computed by using the scheme DSAV with different time steps, where (a) $(\sigma_{12}, \sigma_{13}, \sigma_{23}) = (1, 1, 1)$ and (b) $(\sigma_{12}, \sigma_{13}, \sigma_{23}) = (1, 3, 1)$ (In (b), we append a small inset figure to show the energy evolution computed with the stabilizer $S = 0$).

effectiveness of the stabilization term S in improving energy stability. This kind of phenomenon (with and without stabilizer) had been also reported in [5,7,77,81–89] for the IEQ, SAV, convex-splitting methods, etc.

In Fig. 4.3, we plot the time evolution curves of the original energy (2.3) and the modified energy (3.93) for $(\sigma_{12}, \sigma_{13}, \sigma_{23}) = (1, 1, 1)$ and $(1, 3, 1)$ computed by using the time step size $\delta t = 0.01/2^3$. These two energy curves have always coincided. We impose the profiles of $\frac{1}{2}\phi_1 + \phi_2$ at the initial moment and the steady state in each subfigure. It can be seen that the two bubbles squeeze together for the partial spreading case, while one bubble is absorbed into the other for the total spreading case.

4.2. Liquid lens between two stratified fluids

In this example, we study how the contact angles formed between a liquid lens and the fluid layer of two stratified fluids are affected by different surface tension parameters in 2D. The initial conditions of the three phase-field variables are set respectively as a circular lens and two stratified fluids, where the circular lens is located in the middle of the two stratified fluids, see also in [1,2,6,7,92].

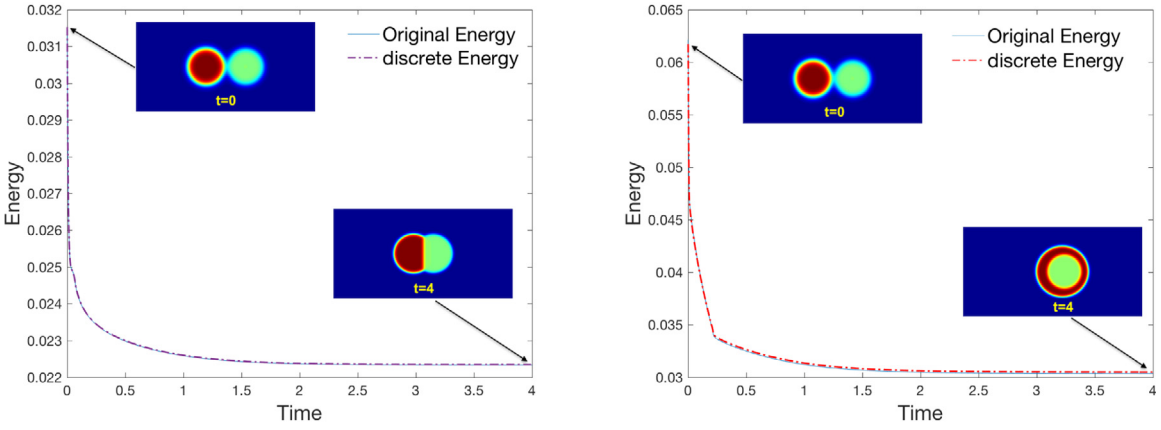

(a) $(\sigma_{12}, \sigma_{13}, \sigma_{23}) = (1, 1, 1)$. (b) $(\sigma_{12}, \sigma_{13}, \sigma_{23}) = (1, 3, 1)$.

Fig. 4.3. The time evolution of the total free energy (2.3) in the original form and (3.93) in the discrete form computed by using the time step $\delta t = 0.01/2^3$ where (a) $(\sigma_{12}, \sigma_{13}, \sigma_{23}) = (1, 1, 1)$ and (b) $(\sigma_{12}, \sigma_{13}, \sigma_{23}) = (1, 3, 1)$. In each subfigure, we append the profile of $\frac{1}{2}\phi_1 + \phi_2$ at the initial moment and the steady state.

We set the computed domain as $(x, y) \in \Omega = [0, 0.7] \times [0, 0.5]$ and the initial conditions read as follows (the profile of $\frac{1}{2}\phi_1^0 + \phi_2^0$ is shown in Fig. 4.4(a) where the region of $\{\phi_i^0 = 1\}$ and the contact angles of θ_i are specified),

$$\begin{cases} \mathbf{u}^0(x, y) = \mathbf{0},\ p^0(x, y) = 0, \\ \phi_1^0(x, y) = (1 - \phi_3^0)\left(\frac{1}{2} + \frac{1}{2}\tanh\left(\frac{4}{\epsilon}(y - 0.25)\right)\right),\ \phi_2^0(x, y) = 1 - \phi_1^0 - \phi_3^0, \\ \phi_3^0(x, y) = \frac{1}{2}\tanh\left(\frac{0.09 - \sqrt{(x - 0.35)^2 + (y - 0.25)^2}}{\epsilon/2}\right) + \frac{1}{2}. \end{cases} \tag{4.3}$$

We assume that the x-direction is periodic, and the y-direction is assumed to satisfy the boundary conditions specified in (2.13). We set the model parameters to

$$M = 10,\ \nu = 1,\ \Lambda = 7,\ \lambda = 0.01,\ B = 10,\ \epsilon = 0.005,\ S = 4,\ \delta t = 1\text{e}{-4},\ h = \frac{1}{512}. \tag{4.4}$$

We use six different surface tension parameter sets, among which $(\sigma_{12}, \sigma_{13}, \sigma_{23}) = (1, 1, 1)$, $(1, 0.6, 0.6)$, $(1, 0.8, 14)$, $(1, 3, 1)$, $(3, 1, 1)$, and $(1, 1, 3)$, where the first three parameter sets are for the partial spreading cases, and the last three parameter sets are for the total spreading cases. In Fig. 4.4(b)–(g), for each case, we plot the steady-state solution for the profile of $\frac{1}{2}\phi_1 + \phi_2$, where we can see the contact lens present various shapes with various contact angles $\theta_1, \theta_2, \theta_3$ (the contact angles are sketched in Fig. 4.4(b)–(d)).

In the limit $\epsilon \to 0$, the relationship between the contact angles of the equilibrium state and three surface tension parameters can be predicted by using Young's relationship (cf. [2,93,94]),

$$\frac{\sin\theta_1}{\sigma_{23}} = \frac{\sin\theta_2}{\sigma_{13}} = \frac{\sin\theta_3}{\sigma_{12}}. \tag{4.5}$$

Theoretical prediction values of the contact angles according to the given surface tension parameters are shown in Table 4.1. We can see that the computed steady-state solutions verify the theoretical prediction of the contact angles. In addition, all these calculations are consistent with the numerical results given in [1,2,5–7], qualitatively.

To verify the consistency between the conserved three-phase Allen–Cahn model and the original three-phase Cahn–Hilliard model developed in [1,2]. In Fig. 4.5, for the three partial spreading cases, we plot the interface contours of $\{\phi_i = 1/2\}$ of the steady-state solutions computed by using these two models, where the original three-phase Cahn–Hilliard model is computed by using the provided nonlinear scheme given in [1,2] with $\delta t = 1\text{e}{-6}$. The interface contours show that there are almost no viewable differences between these two models on the contact angles, which illustrates the effectiveness of the new model.

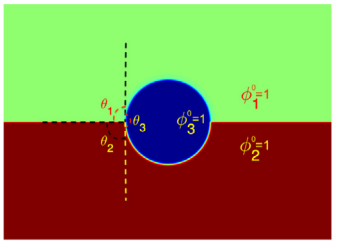

(a) The initial profile of $\frac{1}{2}\phi_1 + \phi_2$.

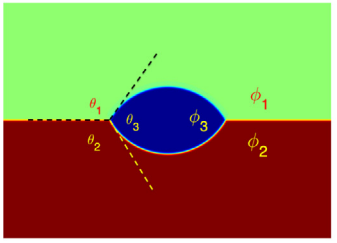

(b) $(\sigma_{12}, \sigma_{13}, \sigma_{23})$=$(1, 1, 1)$.

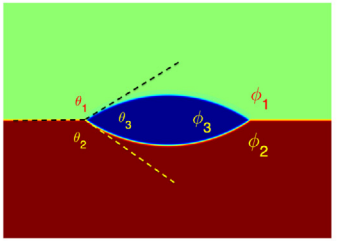

(c) $(\sigma_{12}, \sigma_{13}, \sigma_{23})$=$(1, 0.6, 0.6)$.

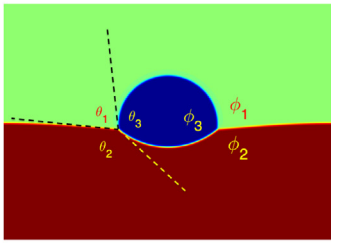

(d) $(\sigma_{12}, \sigma_{13}, \sigma_{23})$=$(1, 0.8, 1.4)$.

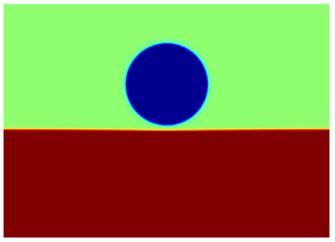

(e) $(\sigma_{12}, \sigma_{13}, \sigma_{23})$=$(1, 1, 3)$.

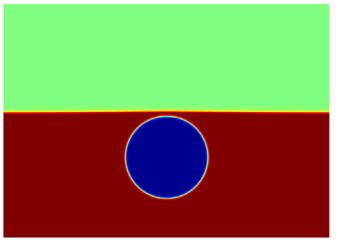

(f) $(\sigma_{12}, \sigma_{13}, \sigma_{23})$=$(1, 3, 1)$.

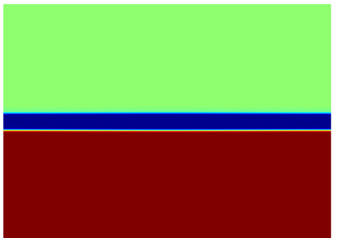

(g) $(\sigma_{12}, \sigma_{13}, \sigma_{23})$=$(3, 1, 1)$.

Fig. 4.4. The initial profile and the steady-state solutions for six surface tension parameters. In each subfigure, we plot the profile of $\frac{1}{2}\phi_1+\phi_2$. (Note: the dashed lines are the approximate tangent lines of the junction point of the numerical solution for each phase-field variable.)

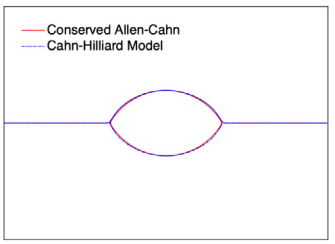

(a) $(\sigma_{12}, \sigma_{13}, \sigma_{23})$=$(1, 1, 1)$.

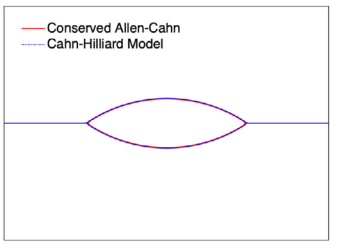

(b) $(\sigma_{12}, \sigma_{13}, \sigma_{23})$=$(1, 0.6, 0.6)$.

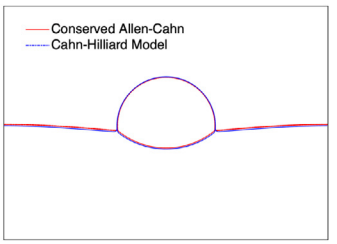

(c) $(\sigma_{12}, \sigma_{13}, \sigma_{23})$=$(1, 0.8, 1.4)$.

Fig. 4.5. Comparison of steady-state solutions of three partial spreading cases calculated using the conserved Allen–Cahn model (2.8)–(2.11) and the ternary Cahn–Hilliard model that is computed by the nonlinear scheme given in [1,2] with $\delta t = 1e{-}6$.

4.3. The dynamics of a rising liquid droplet in 3D

In this example, we simulate the rising and deforming dynamics of a small and light 3D liquid droplet under the action of gravity. For simplicity, the density difference between the rising droplet and the other two fluids is

Table 4.1
Surface tension parameters $(\sigma_{12}, \sigma_{13}, \sigma_{23})$ and the theoretical prediction of contact angles $\theta_1, \theta_2, \theta_3$ derived from Young's relationship (4.5).

$(\sigma_{12}, \sigma_{13}, \sigma_{23})$	(1,1,1)	(1,0.6,0.6)	(1,0.8,1.4)
(partial spreading)	$\theta_1 = \theta_2 = \theta_3$	$\theta_1 = \theta_2 > \theta_3$	$\theta_1 < \theta_3 < \theta_2$
$(\sigma_{12}, \sigma_{13}, \sigma_{23})$	(1,1,3)	(1,3,1)	(3,1,1)
(total spreading)	$\theta_1 = 0, \theta_2 = \theta_3 = \pi$	$\theta_1 = \theta_3 = \pi, \theta_2 = 0$	$\theta_1 = \theta_2 = \pi, \theta_3 = 0$

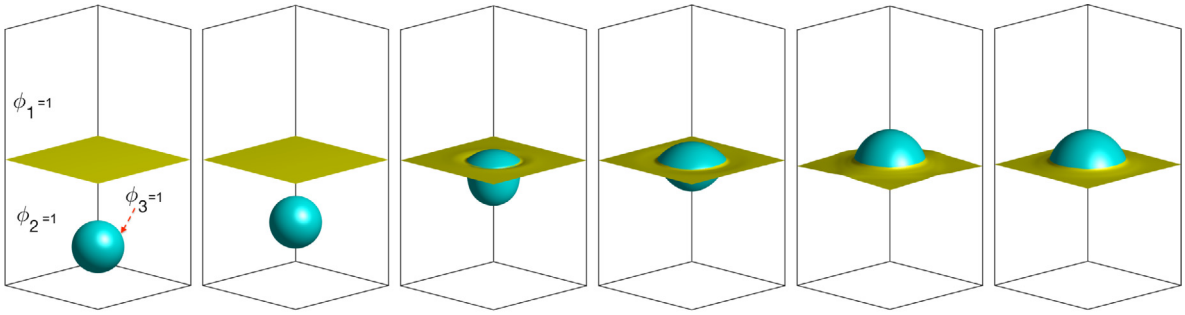

(a) $(\sigma_{12}, \sigma_{13}, \sigma_{23}) = (1, 1, 1)$ with $g_0 = 10$ where snapshots are taken at $t = 0$, 4.2, 10.2, 11, 13.4 and 30.

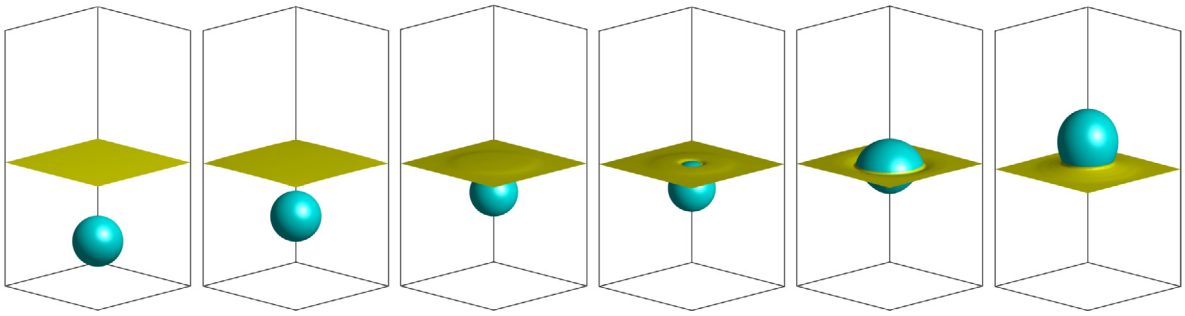

(b) $(\sigma_{12}, \sigma_{13}, \sigma_{23}) = (1, 0.8, 1.4)$ with $g_0 = 10$ where snapshots are taken at $t = 0$, 4.2, 7.8, 8.6, 9.8 and 30.

Fig. 4.6. The dynamics of a 3D rising liquid droplet with two surface tension parameter sets $(\sigma_{12}, \sigma_{13}, \sigma_{23}) = (1, 1, 1)$ and $(1, 0.8, 1.4)$ with the gravity parameter $g_0 = 10$. In each subfigure, snapshots of the isosurfaces $\{\phi_3 = 1/2\}$ (cyan) and $\{\phi_1 = 1/2\}$ (yellow) are plotted.

considered to be relatively small, so we can use the Boussinesq approximation to approximate the gravity force (see also in [26,49,95]). Thus the momentum equation is replaced as follows:

$$\mathbf{u}_t + \mathbf{u} \cdot \nabla \mathbf{u} - \nu \Delta \mathbf{u} + \nabla p + \lambda \sum_{i=1}^{3} \phi_i \nabla \mu_i = \mathbf{g}_0 \phi_3, \tag{4.6}$$

where $\mathbf{g}_0 = (0, 0, g_0)$ and g_0 is the pre-assumed gravity constant.

We set the computational domain as $\Omega = [0, 1] \times [0, 1] \times [0, 2]$, and assume the periodic boundary conditions along the x, y-axes. The boundary conditions along the z-direction are specified in (2.13). The initial condition for these three fluid components are outlined in the first subfigure in Fig. 4.6(a) with the following formulations:

$$\begin{cases} \phi_1^0(x, y, z) = (1 - \phi_3^0)\left(\dfrac{1}{2} + \dfrac{1}{2}\tanh\left(\dfrac{5.5}{\epsilon}(z - 1)\right)\right), \\ \phi_2^0(x, y, z) = 1 - \phi_1^0 - \phi_3^0, \\ \phi_3^0(x, y, z) = \dfrac{1}{2}\tanh\left(\dfrac{0.26 - \sqrt{(x - 0.5)^2 + (y - 0.5)^2 + (z - 0.3)^2}}{\epsilon/2}\right) + \dfrac{1}{2}, \\ \mathbf{u}^0(x, y, z) = (0, 0, 0),\ p^0(x, y, z) = 0. \end{cases} \tag{4.7}$$

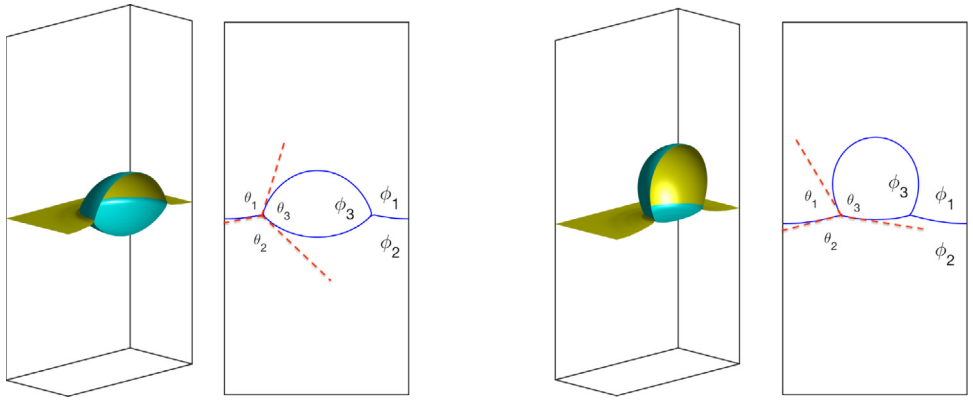

(a) $(\sigma_{12}, \sigma_{13}, \sigma_{23}) = (1, 1, 1)$ (b) $(\sigma_{12}, \sigma_{13}, \sigma_{23}) = (1, 0.8, 1.4)$

Fig. 4.7. Comparisons of the contact angles of steady-state solutions computed using two surface tension parameters. In each subfigure, the left one is the half domain where isosurfaces of $\{\phi_3 = 1/2\}$ (cyan) and $\{\phi_1 = 1/2\}$ (yellow) are plotted, and the right one is the 2D cut plane of $x = 1/2$ where the interface contours of $\{\phi_i = 1/2\}$ are plotted. (Note: the dashed lines are the approximate tangent lines of the junction point of the numerical solution for each phase-field variable.)

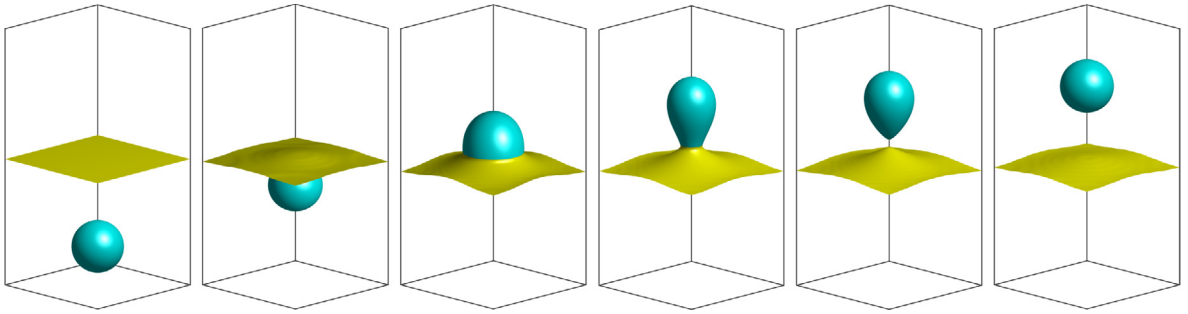

Fig. 4.8. The dynamics of a 3D rising liquid droplet with $(\sigma_{12}, \sigma_{13}, \sigma_{23}) = (1, 1, 1)$ and gravity parameter $g_0 = 20$. Snapshots of the isosurfaces $\{\phi_3 = 1/2\}$ (cyan) and $\{\phi_1 = 1/2\}$ (yellow) are taken at $t = 0$, 5, 9, 16, 17, and 18. (For interpretation of the references to color in this figure legend, the reader is referred to the web version of this article.)

We set the model parameters as

$$M = 1, \nu = 1, \Lambda = 7, B = 10, \epsilon = 0.025, S = 4, \lambda = 0.01, \delta t = 1\text{e}{-3}, h = \frac{1}{256}. \tag{4.8}$$

In Fig. 4.6, we adopt the two sets of surface tension parameters of $(\sigma_{12}, \sigma_{13}, \sigma_{23}) = (1, 1, 1)$ and $(1, 0.8, 1.4)$ with the same gravity parameter of $g_0 = 10$. We use different colors to plot the isosurfaces of $\{\phi_1 = 1/2\}$ (yellow) and $\{\phi_3 = 1/2\}$ (cyan). We find that the droplet is eventually captured by the horizontal interface and floats steadily there. To be able to observe the formed contact angles, in Fig. 4.7, we plot the half computed domain, and a 2D cut-off plane of $x = 1/2$, where the contours of $\{\phi_i = 1/2, i = 1, 2, 3\}$ are plotted. It can be seen that the two sets of surface tension parameters present totally different contact angles, and satisfy the predicted values from Young's relation given in Table 4.1. In Fig. 4.8, we use $(\sigma_{12}, \sigma_{13}, \sigma_{23}) = (1, 1, 1)$ but increase the gravity constant to $g_0 = 20$. We observe that the droplet rises faster and eventually penetrates the horizontal fluid layer to reach the upper part of the computed domain. These 3D results (float/penetrate for low/high gravity) are qualitatively consistent with the 2D simulations using the Cahn–Hilliard three-phase model given in [1].

5. Concluding remarks

The goal of this article includes two folds. We first reformulate the flow-coupled three-component phase-field model using the conserved Allen–Cahn dynamics. Then we develop a novel fully-discrete, second-order time

accurate numerical algorithm with full decoupling structure to solve this highly coupled and nonlinear model. The main idea to design the algorithm is to utilize some special characteristics satisfied by those coupling terms (zero contribution to the dissipation law of energy), and construct several special ODEs, so that the original system is formulated in a form that is conducive for time discretization. By combining with other effective methods for the fluid equations and nonlinear potentials, we arrive at a highly effective scheme that is very easy-to-implement (linear, fully-decoupled), accurate (second-order accuracy in time), and stable (unconditionally energy stability). The implementation is discussed in detail. The rigorous proof of the solvability and unconditional energy stability are presented as well. Through ample numerical simulations, the effectiveness of the model and scheme are demonstrated numerically.

Declaration of competing interest

The authors declare that they have no known competing financial interests or personal relationships that could have appeared to influence the work reported in this paper.

Acknowledgments

Yang's research is partially supported by the U.S. National Science Foundation under grant numbers DMS-1818783 and DMS-2012490. He's research is partially supported by the U.S. National Science Foundation under grant number DMS-1818642.

References

[1] F. Boyer, C. Lapuerta, Study of a three component Cahn–Hilliard flow model, ESAIM: Math. Model. Numer. Anal. 40 (4) (2006) 653–687.
[2] F. Boyer, S. Minjeaud, Numerical schemes for a three component Cahn–Hilliard model, ESAIM: Math. Model. Numer. Anal. 45 (04) (2011) 697–738.
[3] J. Kim, K. Kang, J. Lowengrub, Conservative multigrid methods for ternary Cahn-Hilliard systems, Commun. Math. Sci. 2 (2004) 53–77.
[4] S. Wu, J. Xu, Multiphase Allen-Cahn and Cahn-Hilliard models and their discretizations with the effect of pairwise surface tensions, J. Comput. Phys. 343 (2017) 10–32.
[5] X. Yang, J. Zhao, Q. Wang, J. Shen, Numerical approximations for a three components Cahn-Hilliard phase-field Model based on the Invariant Energy Quadratization method, Math. Models Methods Appl. Sci. 27 (2017) 1993–2030.
[6] J. Zhang, X. Yang, Decoupled, non-iterative, and unconditionally energy stable large time stepping method for the three-phase Cahn-Hilliard phase-field model, J. Comput. Phys. 404 (2020) 109115.
[7] J. Zhang, X. Yang, Unconditionally energy stable large time stepping method for the L2-gradient flow based ternary phase-field model with precise nonlocal volume conservation, Comput. Methods Appl. Mech. Engrg. 361 (2020) 112743.
[8] W. Chen, C. Wang, S. Wang, X. Wang, S.M. Wise, Energy stable numerical schemes for ternary Cahn-Hilliard system, J. Sci. Comput. 84 (2020) 27.
[9] J.L. Guermond, P. Minev, J. Shen, An Overview of Projection methods for incompressible flows, Comput. Methods Appl. Mech. Engrg. 195 (2006) 6011–6045.
[10] J.L. Guermond, L. Quartapelle, A projection FEM for variable density incompressible flows, J. Comput. Phys. 165 (1) (2000) 167–188.
[11] J.L. Guermond, A. Salgado, A splitting method for incompressible flows with variable density based on a pressure Poisson equation, J. Comput. Phys. 228 (8) (2009) 2834–2846.
[12] J.-L. Guermond, A. Salgado, Error analysis of a fractional time-stepping technique for incompressible flows with variable density, SIAM J. Numer. Anal. 49 (3) (2011) 917–944.
[13] R. Nochetto, J.-H. Pyo, The Gauge-Uzawa finite element method part I: the Navier-Stokes equations, SIAM J. Numer. Anal. 43 (2005) 1043–1068.
[14] J. Pyo, J. Shen, Gauge-Uzawa methods for incompressible flows with variable density, J. Comput. Phys. 221 (2007) 181–197.
[15] J. Shen, X. Yang, A phase-field model and its numerical approximation for two-phase incompressible flows with different densities and viscositites, SIAM J. Sci. Comput. 32 (2010) 1159–1179.
[16] A. Diegel, C. Wang, X. Wang, S. Wise, Convergence analysis and error estimates for a second order accurate finite element method for the Cahn-Hilliard-Navier-Stokes system, Numer. Math. 137 (2017) 495–534.
[17] X. Feng, Fully discrete finite element approximations of the Navier-Stokes-Cahn-Hilliard diffuse interface model for two-phase fluid flows, ESAIM: Math. Model. Numer. Anal. 44 (2006) 1049–1072.
[18] D. Han, A. Brylev, X. Yang, Z. Tan, Numerical analysis of second order, fully discrete energy stable schemes for phase field models of two phase incompressible flows, J. Sci. Comput. 70 (2017) 965–989.
[19] D. Han, X. Wang, A second order in time, uniquely solvable, unconditionally stable numerical scheme for Cahn-Hilliard-Navier-Stokes equation, J. Comput. Phys. 290 (2015) 139–156.

[20] D. Han, X. Wang, A second order in time, decoupled, unconditionally stable numerical scheme for the Cahn-Hilliard-Darcy system, J. Sci. Comput. 14 (2018) 1210–1233.
[21] X. Yang, Efficient and Energy Stable scheme for the hydrodynamically coupled three components Cahn-Hilliard phase-field model using the stabilized-Invariant Energy Quadratization (S-IEQ) approach, J. Comput. Phys. 438 (2021) 110342.
[22] X. Yang, Efficient, Second-order in time, and Energy Stable scheme for a new hydrodynamically coupled three components volume-conserved Allen-Cahn phase-field model, Math. Models Methods Appl. Sci. 31 (4) (2021) 753–787.
[23] D. Kay, V. Styles, R. Welford, Finite element approximation of a Cahn-Hilliard-Navier-Stokes system, Interfaces Free Bound. 10 (2008) 15–43.
[24] C. Liu, J. Shen, X. Yang, Decoupled energy stable schemes for a phase-field model of two-phase incompressible flows with variable density, J. Sci. Comput. 62 (2015) 601–622.
[25] S. Minjeaud, An unconditionally stable uncoupled scheme for a triphasic Cahn–Hilliard/Navier–Stokes model, Numer. Methods Partial Differential Equations 29 (2013) 584–618.
[26] J. Shen, X. Yang, Decoupled energy stable schemes for phase filed models of two phase complex fluids, SIAM J. Sci. Comput. 36 (2014) B122–B145.
[27] J. Shen, X. Yang, Decoupled, energy stable schemes for phase-field models of two-phase incompressible flows, SIAM J. Numer. Anal. 53 (1) (2015) 279–296.
[28] X. Yang, A new efficient Fully-decoupled and Second-order time-accurate scheme for Cahn-Hilliard phase-field model of three-phase incompressible flow, Comput. Methods Appl. Mech. Engrg. 376 (2021) 113589.
[29] J. Rubinstein, P. Sternberg, Nonlocal reaction-diffusion equations and nucleation, IMA J. Appl. Math. 48 (1992) 249–264.
[30] D.C. Antonopoulou, P.W. Bates, D. Blomker, G.D. Karali, Motion of a droplet for the stochastic mass-conserving Allen-Cahn equation, SIAM J. Math. Anal. 48 (2016) 670–708.
[31] Z. Chai, D. Sun, H. Wang, B. Shi, A comparative study of local and nonlocal Allen-Cahn equations with mass conservation, Int. J. Heat Mass Transfer 122 (2018) 631–642.
[32] X. Chen, D. Hilhorst, E. Logak, Mass conserved Allen-Cahn equation and volume preserving mean curvature flow , Interfaces Free Bound. 12 (2010) 527–549.
[33] P.-H. Chiu, Y.-T. Lin, A conservative phase field method for solving incompressible two-phase flows, J. Comput. Phys. 230 (1) (2011) 185–204.
[34] D. Jeong, J. Kim, Conservative Allen-Cahn-Navier-Stokes system for incompressible two-phase fluid flows, Comput. & Fluids 156 (2017) 239–246.
[35] J. Kim, S. Lee, Y. Choi, A conservative Allen-Cahn equation with a space-time dependent Lagrange multiplier, Internat. J. Engrg. Sci. 84 (2014) 11–17.
[36] P.E. Kettani, D. Hilhorst, K. Lee, A stochastic mass conserved reaction-diffusion equation with nonlinear diffusion, Discrete Contin. Dyn. Syst. Ser. A 38 (2018) 5615–5648.
[37] F. Lin, X.-M. He, X. Wen, Fast, unconditionally energy stable large time stepping method for a new Allen-Cahn type square phase-field crystal model, Appl. Math. Lett. 92 (2019) 248–255.
[38] J. Vaibhav, K.J. Rajeev, An adaptive variational procedure for the conservative and positivity preserving Allen-Cahn phase-field model, J. Comput. Phys. 366 (2018) 478–504.
[39] J. Vaibhav, K.J. Rajeev, A positivity preserving and conservative variational scheme for phase-field modeling of two-phase flows, J. Comput. Phys. 360 (2018) 137–166.
[40] A. Baskaran, P. Zhou, Z. Hu, C. Wang, Energy stable and efficient finite-difference nonlinear multigrid schemes for the modified phase field crystal equation, J. Comput. Phys. 250 (2013) 270–292.
[41] Y. Qin, C. Wang, Z. Zhang, A positivity-preserving and convergent numerical scheme for the binary fluid-surfactant system, Int. J. Numer. Anal. Model. 18 (2021) 399–425.
[42] S.M. Wise, C. Wang, J.S. Lowengrub, An energy-stable and convergent finite-difference scheme for the phase field crystal equation, SIAM J. Numer. Anal. 47 (3) (2009) 2269–2288.
[43] C. Wang, S.M. Wise, An energy stable and convergent finite-difference scheme for the modified phase field crystal equation, SIAM J. Numer. Anal. 49 (2011) 945–969.
[44] Z. Hu, S.M. Wise, C. Wang, J.S. Lowengrub, Stable and efficient finite difference nonlinear-multigrid schemes for the phase field crystal equation, J. Comput. Phys. 228 (2009) 5323–5339.
[45] J. Yang, S. Mao, X.-M. He, X. Yang, Y. He, A diffuse interface model and semi-implicit energy stable finite element method for two-phase magnetohydrodynamic flows, Comput. Methods Appl. Mech. Engrg. 356 (2019) 435–464.
[46] H. Gomez, X. Nogueira, An unconditionally energy-stable method for the phase field crystal equation, Comput. Methods Appl. Mech. Engrg. 249–252 (2012) 52–61.
[47] Q. Huang, X. Yang, X.-M. He, Numerical approximations for a smectic-A liquid crystal flow model: first-order, linear, decoupled and energy stable schemes, Discrete Contin. Dyn. Syst. Ser. B 23 (6) (2018) 2177–2192.
[48] C. Xu, T. Tang, Stability analysis of large time-stepping methods for epitaxial growth models, SIAM J. Numer. Anal. 44 (2006) 1759–1779.
[49] X. Yang, J.J. Feng, C. Liu, J. Shen, Numerical simulations of jet pinching-off and drop formation using an energetic variational phase-field method, J. Comput. Phys. 218 (2006) 417–428.
[50] C. Xu, C. Chen, X. Yang, X.-M. He, Numerical approximations for the hydrodynamics coupled binary surfactant phase field model: second order, linear, unconditionally energy stable schemes, Commun. Math. Sci. 17 (3) (2019) 835–858.
[51] X. Yang, D. Han, Linearly first- and second-order, unconditionally energy stable schemes for the phase field crystal equation, J. Comput. Phys. 330 (2017) 1116–1134.

[52] X. Yang, J. Zhao, X.-M. He, Linear, second order and unconditionally energy stable schemes for the viscous Cahn-Hilliard equation with hyperbolic relaxation using the invariant energy quadratization method, J. Comput. Appl. Math. 343 (1) (2018) 80–97.
[53] J. Zhang, X. Yang, On Efficient numerical schemes for a two-mode phase field crystal model with face-centered-cubic (FCC) ordering structure, Appl. Numer. Math. 146 (2019) 13–37.
[54] J. Zhang, X. Yang, Numerical approximations for a new L2-gradient flow based phase field crystal model with precise nonlocal mass conservation, Comput. Phys. Comm. 243 (2019) 51–67.
[55] J. Zhang, X. Yang, Efficient and accurate numerical scheme for a magnetic-coupled phase-field-crystal model for ferromagnetic solid materials, Comput. Methods Appl. Mech. Engrg. 371 (2020) 113110.
[56] A. Diegel, X. Feng, S. Wise, Analysis of a mixed finite element method for a Cahn-Hilliard-Darcy-Stokes system, SIAM J. Numer. Anal. 53 (1) (2015) 127–152.
[57] X. Feng, Fully discrete finite element approximations of the Navier-Stokes-Cahn-Hilliard diffuse interface model for two-phase fluid flows, SIAM J. Numer. Anal. 44 (3) (2006) 1049–1072.
[58] X. Feng, Y. He, C. Liu, Analysis of finite element approximations of a phase field model for two-phase fluids, Math. Comp. 76 (258) (2007) 539–571.
[59] X. Feng, Y. Li, Analysis of symmetric interior penalty discontinuous Galerkin methods for the Allen-Cahn equation and the mean curvature flow, IMA J. Numer. Anal. 35 (4) (2015) 1622–1651.
[60] X. Feng, Y. Li, Y. Xing, Analysis of mixed interior penalty discontinuous Galerkin methods for the Cahn-Hilliard equation and the Hele-Shaw flow, SIAM J. Numer. Anal. 54 (2) (2016) 825–847.
[61] X. Feng, S. Wise, Analysis of a Darcy-Cahn-Hilliard diffuse interface model for the Hele-Shaw flow and its fully discrete finite element approximation, SIAM J. Numer. Anal. 50 (3) (2012) 1320–1343.
[62] Y. Gao, X.-M. He, L. Mei, X. Yang, Decoupled, linear, and energy stable finite element method for the Cahn-Hilliard-Navier-Stokes-Darcy phase field model, SIAM J. Sci. Comput. 40 (1) (2018) B110–B137.
[63] Y. Gao, X.-M. He, Y. Nie, Second-order, fully decoupled, linearized, and unconditionally stable SAV schemes for Cahn-Hilliard-Darcy system, Numer. Methods Partial Differential Equations (2021) http://dx.doi.org/10.1002/num.22829.
[64] R. Li, Y. Gao, J. Chen, L. Zhang, X.-M. He, Z. Chen, Discontinuous finite volume element method for a coupled Navier-Stokes-Cahn-Hilliard phase field model, Adv. Comput. Math. 46 (2020) #25.
[65] R. Nochetto, A. Salgado, I. Tomas, A diffuse interface model for two-phase ferrofluid flows, Comput. Methods Appl. Mech. Engrg. 309 (2016) 497–531.
[66] R. Nochetto, A. Salgado, S. Walker, A diffuse interfce model for electrowetting with moving contat lines, Math. Models Methods Appl. Sci. 24 (1) (2014) 67–111.
[67] L. Rebholz, S. Wise, M. Xiao, Penalty-projection schemes for the Cahn-Hilliard Navier-Stokes diffuse interface model of two phase flow, and their connection to divergence-free coupled schemes, Int. J. Numer. Anal. Model. 15 (2018) 649–676.
[68] G. Zhang, X.-M. He, X. Yang, Decoupled, linear, and unconditionally energy stable fully-discrete finite element numerical scheme for a two-phase ferrohydrodynamics model, SIAM J. Sci. Comput. 43 (1) (2021) B167–B193.
[69] G. Zhang, X.-M. He, X. Yang, A fully decoupled linearized finite element method with second-order temporal accuracy and unconditional energy stability for incompressible MHD equations, J. Comput. Phys. (2021) http://dx.doi.org/10.1016/j.jcp.2021.110752.
[70] R.H. Nochetto, A.J. Salgado, I. Tomas, A diffuse interface model for two-phase ferrofluid flows, Comput. Methods Appl. Mech. Engrg. 309 (2016) 497–531.
[71] B.I. Lev, V.G. Nazarenko, A.B. Nych, P.M. Tomchuk, Deformation and instability of nematic drops in an external electric field, JETP Lett. 71 (2000) 262–265.
[72] R.H. Nochetto, A.J. Salgado, S.W. Walker, A diffuse interface model for electrowetting with moving contact lines, Math. Models Methods Appl. Sci. 24 (2014) 67–111.
[73] F. Bai, D. Han, X.-M. He, X. Yang, Deformation and coalescence of ferrodroplets in Rosensweig model using the phase field and modified level set approaches under uniform magnetic fields, Commun. Nonlinear Sci. Numer. Simul. 85 (2020) 105213.
[74] F. Bai, X.-M. He, R. Zhou, X. Yang, C. Wang, Three dimensional phase-field investigation of droplet formation in microfluidic flow focusing devices with experimental validation, Int. J. Multiph. Flow. 93 (2017) 130–141.
[75] D. Han, X.-M. He, Q. Wang, Y. Wu, Existence and weak-strong uniqueness of solutions to the Cahn-Hilliard-Navier-Stokes-Darcy system in superposed free flow and porous media, Nonlinear Anal. 211 (2021) #112411.
[76] D. Han, X. Wang, H. Wu, Existence and uniqueness of global weak solutions to a Cahn-Hilliard-Stokes-Darcy system for two phase incompressible flows in karstic geometry, J. Differential Equations 257 (10) (2014) 3887–3933.
[77] J. Shen, X. Yang, The IEQ and SAV approaches and their extensions for a class of highly nonlinear gradient flow systems, Contemp. Math. 754 (2020) 217–245.
[78] V. Girault, P.A. Raviart, Finite Element Method for Navier-Stokes Equations: Theory and Algorithms, Springer-Verlag, Berlin, Heidelberg, 1987, pp. 395–414.
[79] J. Shen, On error estimates of the projection methods for the Navier-Stokes equations: second-order schemes, Math. Comp. 65 (215) (1996) 1039–1065.
[80] W. E, J.G. Liu, Projection method. I. Convergence and numerical boundary layers, SIAM J. Numer. 32 (1995) 1017–1057.
[81] C. Chen, X. Yang, Fast, provably unconditionally energy stable, and second-order accurate algorithms for the anisotropic Cahn-Hilliard model, Comput. Methods Appl. Mech. Engrg. 351 (2019) 35–59.
[82] J. Shen, J. Xu, J. Yang, A new class of efficient and robust energy stable schemes for gradient flows, SIAM Rev. 61 (2019) 474–506.
[83] J. Shen, J. Xue, J. Yang, The scalar auxiliary variable (SAV) approach for gradient flows, J. Comput. Phys. 353 (2018) 407–416.
[84] Z. Yang, S. Dong, An unconditionally energy-stable scheme based on an implicit auxiliary energy variable for incompressible two-phase flows with different densities involving only precomputable coefficient matrices, J. Comput. Phys. 393 (2018) 229–257.

[85] C. Chen, X. Yang, Efficient numerical scheme for a dendritic solidification phase field model with melt convection, J. Comput. Phys. 388 (2019) 41–62.
[86] K. Cheng, C. Wang, S.M. Wise, An energy wtable BDF2 Fourier pseudo-spectral numerical scheme for the square phase field crystal equation, Comm. Comput. Phys. 26 (2019) 1335–1364.
[87] J. Shen, X. Yang, Numerical approximations of Allen–Cahn and Cahn–Hilliard equations, Discrete Contin. Dyn. Syst. A 28 (2010) 1669–1691.
[88] X. Yang, Linear, first and second order and unconditionally energy stable numerical schemes for the phase field model of homopolymer blends, J. Comput. Phys. 327 (2016) 294–316.
[89] X. Yang, H. Yu, Efficient second order unconditionally stable schemes for a phase field moving contact line model using an invariant energy quadratization approach, SIAM J. Sci. Comput. 40 (2018) B889–B914.
[90] R. Ingram, A new linearly extrapolated crank-nicolson time-stepping scheme for the Navier-Stokes equations, Math. Comp. 82 (284) (2013) 1953–1973.
[91] J. van Kan, A second-order accurate pressure-correction scheme for viscous incompressible flow, SIAM J. Sci. Stat. Comput. 7 (3) (1986) 870–891.
[92] F. Boyer, C. Lapuerta, S. Minjeaud, B. Piar, M. Quintard, Cahn-Hilliard/Navier-Stokes model for the simulation of three-phase flows, Transp. Porous Media 82 (2010) 463–483.
[93] J. Kim, J. Lowengrub, Phase field modeling and simulation of three-phase flows, Interfaces Free Bound. 7 (2005) 435–466.
[94] J.S. Rowlinson, B. Widom, Molecular Theory of Capillarity, Clarendon Press, Oxford, 1989.
[95] T. Qin, S. Ragab, P. Yue, Axisymmetric simulation of the interaction of a rising bubble with a rigid surface in viscous flow, Int. J. Multiph. Flow. 52 (2013) 60–70.